CREWES

Research Report 2018
Volume 30

In this volume…

Report Summaries

*For **Complete Reports** and **Student Theses** please visit:*

https://www.crewes.org

(Sign in/password required)

UNIVERSITY OF CALGARY
FACULTY OF SCIENCE
Department of Geoscience

Notice of Intent to Publish

Please note that the authors of the research in this 30th Volume of the Abstract Book intend to publish or otherwise publically disseminate their full research papers in the coming calendar year. According to the contracts between the University of Calgary (CREWES) and each Sponsor, the University will make available to the Sponsor a copy of the proposed publication resulting from the CREWES Project prior to submission for publication. In the event that the Sponsor determines that Research Results within the proposed publication contain Sponsor Confidential Information, the Sponsor shall have thirty (30) days to notify the University in writing and the University shall remove Sponsor Confidential information prior to publication. This 30 day period shall be considered to have started at the end of this meeting (December 1, 2018). These full research reports are available on the CREWES website to all Sponsors and their employees.

For Roy

The greatness of an individual can be gauged by many measures. Two of these are the individual's influence on others and their treatment of people who do not have authority over them. By both measures, Roy Lindseth must be considered a great geophysicist. In his classic 1979 Geophysics paper "Synthetic sonic logs", Roy showed how seismic impedance could be estimated by utilizing seismic reflections amplitudes and well log data. Lindseth's Seislog method is still used by seismic inversion practitioners to this day. Lindseth's contributions led to him receiving SEG's highest award, the Maurice Ewing Medal. Even during retirement from the work force, Roy never retired from geophysics or interest in geophysicists. Roy would come to the University of Calgary on Fridays to hear talks by graduate students in CREWES. Roy volunteered to edit CREWES reports of these students and he attended the annual sponsors meeting for many years prior to his passing in 2018. Unsolicited generosity was characteristic of Roy Lindseth throughout his long and storied research career. Roy Lindseth was truly a Canadian geophysical icon. He was a gentleman, a scholar, a successful entrepreneur, a philanthropist and a great Canadian. We will miss him very much.

Larry Lines
Professor, Department of Geoscience, University of Calgary.

CREWES in 2018

It is once again my distinct pleasure to welcome you to the CREWES Annual Sponsor's Meeting and technical review. 2018 marks the 30th year CREWES has been carrying out seismic research, and I don't think we are going to disappoint.

I'm proud of and amazed at the range and depth of the ideas, applications, and experiments represented in these reports. A quick glance through these pages will show you new thinking in multi-parameter waveform inversion methods for land and unconventional reservoir monitoring; new uses, processing, and acquisition methodologies for DAS fibreoptic data; new ways of formulating and applying compressive sensing and least-squares imaging; new applications of machine learning and deep learning. We've been pushing forward this year with our ongoing program – which is to do the basic and applied science necessary for these new and extended technologies to be brought online.

In 2018 we carried out the first major field campaign of the last few years, partnering with INOVA, High Definition Seismic Corporation, Fotech, Halliburton, Moncur Groundwater, GPUSA and the CaMI-FRS to create some world firsts. The main data set is a walkaway-walkaround VSP into over 300 3C phones, as well as straight and helical-wound DAS fibre in the CaMI geophysics observation well at the Newell County Field Research Station. This data set contains years worth of research in it; its immediate use will be to support multiparameter full waveform inversion with viscoelasticity and anisotropy included, and to support our examination of how DAS and 3C data complement one another in modern applications such as FWI. At the same time we designed and deployed a prototype multicomponent DAS array to carry out field-testing of 6C DAS sensing; CaMI and CREWES collaborated in the testing of a permanent source installment at the FRS, and testing of a land shear streamer.

We are delighted to once again be working with Joe Wong, who has returned to support and lead extensions of the physical modeling laboratory. The lab has been working overtime in the last few months, supporting new benchmark data acquisitions for microseismic and seismic-while-drilling studies. Amongst the improvements are additional digitizers (improving acquisition rate), new S-wave transducers, and adaptations of the source encoding to permit more complex source signatures (e.g., drillstring signatures, microseismic sources, and even seismic traces to be fed back into the medium).

This year we are trying something a little different for our post-meeting Saturday short course. We are going to do a full day course, co-taught by our postdoctoral fellow cohort, on the ideas, algorithms, and applications of Machine Learning. The course is designed to be experiential: your hands will get dirty (well, covered in bytes, anyway) as you take part and even compete amongst each other in training ML tools to recognize features of and take action on seismic and well data.

The research and training activities carried out by CREWES can only happen because of your support and the support of your companies. Your dollars are critically important. We realize how difficult it is, and how hard you work, to champion CREWES at your home companies and institutions, and to ensure that the dollars keeping it going continue to flow. For that, on behalf of all of us, thank you. In return, we once again commit in 2019 to generating the kind of results that make your job an easier one!

Calgary, Alberta — Kristopher Innanen
November, 2018 — CREWES Director

Table of Contents

* Oral Presenter † Poster Presenter

2018 CREWES Sponsors

Acceleware

CGG

Chevron Corporation

Devon Energy Corporation

Halliburton

INOVA Geophysical

Nexen Energy ULC

Petronas Carigali SDN BHD

Repsol Oil & Gas Canada Inc.

RIPED, PetroChina

Saudi Aramco

Sinopec

TGS

Natural Sciences and Engineering Research Council of Canada (NSERC) - Collaborative Research and Development Grant

NSERC CRSNG

Additional funding provided by:

CANADA FIRST RESEARCH EXCELLENCE FUND

Mitacs

CREWES Personnel 2018

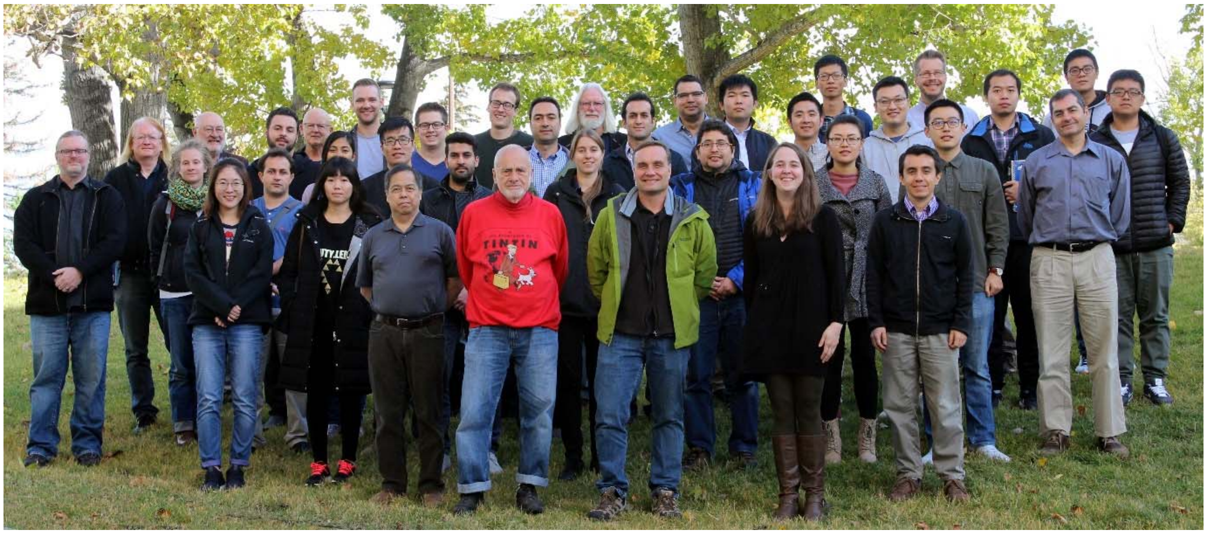

LEADERSHIP

Kris Innanen, Director
Associate Professor, Department of Geoscience, University of Calgary

B.Sc. Physics and Earth Science, 1996, York University
M.Sc. Physics, 1998, York University
Ph.D. Geophysics, 2003, University of British Columbia

- Work Experience: University of Houston

Don C. Lawton, Associate Director
Professor, Department of Geoscience, University of Calgary

B.Sc. (Hons. Class I) Geology, 1973, University of Auckland
Ph.D. Geophysics, 1979, University of Auckland

- Work Experience: New Zealand Steel Mining Ltd., Amoco Minerals (N.Z.) Ltd., Carbon Management Canada

Daniel Trad, Associate Director
Associate Professor, Department of Geoscience, University of Calgary

Licenciatura in Geophysics, 1994, Universidad Nacional de San Juan, Argentina
Ph.D Geophysics, 2001, University of British Columbia

- Work Experience: Electromagnetic Methods (Argentina and Brazil), Seismic Research and development (Veritas, CGG, Techco, in Calgary and France)

Michael P. Lamoureux
Professor, Department of Mathematics and Statistics, University of Calgary
Adjunct Professor, Department of Geoscience, University of Calgary

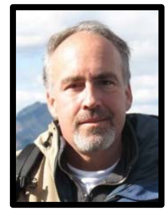

B.Sc. Mathematics, 1982, University of Alberta
M.Sc. Mathematics, 1983, Stanford University
Ph.D. Mathematics, 1988, University of California, Berkeley

- Work Experience: Farallon Computing, NSERC Canada

Kevin W. Hall, Technical Manager

B.Sc. Geophysics, 1992, University of Calgary
M.Sc. Geophysics, 1996, University of Calgary

- Work Experience: Lithoprobe Seismic Processing Facility at the University of Calgary

Gary F. Margrave, Emeritus Director
Emeritus Professor, Faculty Professor, Department of Geoscience, University of Calgary

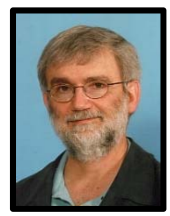

B.Sc. Physics, 1975, University of Utah
M.Sc. Physics, 1977, University of Utah
Ph.D. Geophysics, 1981, University of Alberta

- Work Experience: Chevron Canada Resources, Chevron Geoscience Company, Devon Canada

Laurence R. Lines, Emeritus Director
Professor, Department of Geoscience, University of Calgary

B.Sc. Physics, 1971, University of Alberta
M.Sc. Geophysics, 1973, University of Alberta
Ph.D. Geophysics, 1976, University of B.C.

- Work Experience: Amoco Production Research, Tulsa University, Memorial University of Newfoundland

RESEARCH STAFF, POST DOCS AND VISITING SCHOLARS

Kevin L. Bertram

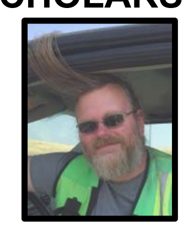

Electronics Technician Certificate, 2005, Southern Alberta Institute of Technology

- Work Experience: Aram Systems Ltd.

Malcolm Bertram

B.Sc. Geology, Auckland, New Zealand

- Work Experience: GSI (Western Australia), Western Geophysics (Western Australia), Auckland University, University of Calgary

Huaizhen Chen

B.Sc. Geophysics, 2010, China University of Petroleum
Ph.D. Geophysics, 2015, China University of Petroleum

Raúl Cova

B.Sc. Geophysical Engineering, 2004. Simon Bolivar University, Venezuela
Ph.D. Geopysics, 2017, University of Calgary
Graduate Diploma in Petroleum Studies, 2011, IFP School, Venezuela

- Work experience: PDVSA Intevep. Venezuela, Shell Canada

Marcelo Guarido de Andrade

B.Sc. Physics, 2006, University of São Paulo, Brazil
M.Sc. Geophysics, 2008, University of São Paulo, Brazil
Ph.D. Geophysics, 2017, University of Calgary

- Work Experience: Schlumberger (Houston), PGS (Rio de Janeiro, Brazil), Orthogonal Geophysics, Husky Energy

David C. Henley

B.Sc. Physics, 1967, Colorado State University
M.Sc. Physics, 1968, University of Michigan

- Work Experience: Shell Oil Co., Shell Canada Ltd.

Helen Isaac

B.Sc. Mathematics, 1973, Imperial College, London
M.Sc. Geophysics, 1974, Imperial College, London
Ph.D. Geophysics, 1996, University of Calgary

- Work Experience: Phillips Petroleum Company, Hudson's Bay Oil and Gas, Canterra Energy, Husky, Fold-Fault Research Project at the University of Calgary

Junxiao Li

B.Sc. Science of Information and Computing (Geophysics), 2009, China University of Petroleum (Beijing)
B.A. English, 2009, China University of Petroleum (Beijing)
M.Sc. Geophysics, 2012, China University of Petroleum (Beijing)
Ph.D. Geophysics, 2017, University of Calgary

Marie Macquet

B.Sc. Earth Science, 2009, University of Nantes (France)
M.Sc. Planetology, 2011, University of Nantes (France)
Ph.D. Geophysics, 2014, Isterre, University of Grenoble (France)

Shahpoor Moradi

B.Sc. Applied Physics, 2000, University of Razi, Iran
M.Sc. Theoretical Physics, 2002, University of Razi, Iran
Ph.D. Theoretical Physics, 2006, University of Razi, Iran
Ph.D. Geophysics, 2017, University of Calgary

Jian Sun

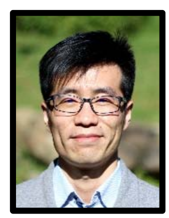

B.Sc. Geophysics, 2009, Shandong University of Science and Technology, China
M.Sc. Geophysics, 2012, Shandong University of Science and Technology, China
Ph.D. Geophysics, 2013, China University of Geosciences (Beijing), China
Ph.D. Geophysics, 2018, University of Calgary

GRADUATE STUDENTS

Hussain Aldhaw

B.Sc. Geosciences, 2012, University of Tulsa, Oklahoma

- Work Experience: Saudi Aramco

Tim Cary

B.A. in Physics, 2012, University of Oxford
B.Sc. in Geophysics with distinction, 2016, University of Calgary

- Work experience: Imperial Oil, Nexen Energy UCL

Matt Eaid

B.Sc. (First Class Honours) Geophysics,2015, University of Calgary

- Work experience: Shell Canada Ltd., Husky Energy

Dennis Ellison

B.Sc. Geophysics, 2013, University of Calgary

- Work experience: Thrust Belt Imaging, Devon Energy Corporation

Ali Fathalian

B.Sc. Applied Physics, 2001, University of Razi, Iran
M.Sc. Condensed Matter Physics, 2003, University of Razi, Iran
Ph.D. Condensed Matter Physics, 2007, University of Razi, Iran

Xin Fu

B.Sc. Geophysics, 2015, China University of Petroleum (East China)
M.Sc. Geophysics, 2018, China University of Petroleum(Beijing)

Adriana Gordon

B.Sc. Geophysics 2015, Simon Bolivar University, Venezuela

- Work Experience: Nexen Energy ULC

Heather Hardeman-Vooys

B.Sc. Mathematics (summa cum laude), 2012, University of Montevallo, AL, USA
M.A. Mathematics, 2014, Wake Forest University, NC, USA.

- Work Experience: Fotech Solutions

Qi Hu

B.Sc. Geophysics, 2011, Yangtze University, Hubei, China
M.Sc. Geophysics, 2014, China University of Petroleum, China

- Work Experience: Sinopec Geophysical Research Institute

Shang Huang

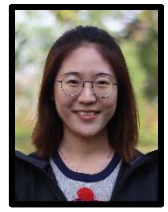

B.Eng. Geophysics, 2017, China University of Petroleum, China
M.Sc. Geophysics, 2018, University of Calgary

Nadine Igonin

B.Sc. Geophysics (First Class Honours), 2016, University of Calgary

- Work Experience: Microseismic Industry Consortium at the University of Calgary

Andy Iverson

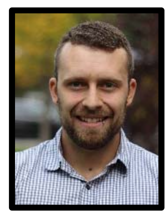

B.Sc. Geophysics (First Class Honours), 2012, University of Calgary

- Work Experience: Apache Canada Ltd, Nexen Energy ULC, Velvet Energy Ltd.

Scott Keating

B.Sc. Honours Physics, 2014, University of Alberta

Bernie Law

B.Sc. Geological Engineering (Geophysics), 1982, University of Saskatchewan

- Work Experience: Key Seismic Solutions Ltd.

Arthur Lee

B.Sc. in Electrical Engineering (minor in Computer Engineering), 1988, University of Calgary

- Work Experience: Hampson-Russell GeoSoftware CGG Calgary

Da Li

B.Sc. Geophysics, 2012, China University of Geosciences (Beijing)
M.Sc. Geophysics, 2016, China University of Geosciences (Beijing)

Ellen Liu

B.Sc. Chemical Engineering, 2014, University of Alberta

- Work Experience: ConocoPhillips Canada

Jorge Monsegny

B.Sc. Computer Science, 2003, National University of Colombia
M.Sc. Mathematics, 2007, National University of Colombia

- Work Experience: Santander Industrial University, Ecopetrol ICP, National University of Colombia

Zhan Niu

B.Sc. Geophysics (Honor degree with minor in geology), 2017, University of Calgary

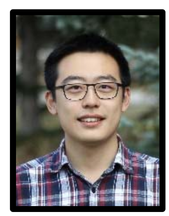

Luping Qu

B.Sc. Geophysics, 2014, China University of Petroleum (East China)
M.Sc. Geophysics, 2017, China University of Petroleum (Beijing)

Sergio Jorge Romahn Reynoso

B. Eng. Geophysics, 2004, National University of Mexico
M.Sc. Exploration Geophysics, 2012, University of Leeds. U.K.

- Work Experience: PEMEX

Tyler Spackman

B.Sc. in Geophysics with distinction 2014, University of Calgary

- Work Experience: Tourmaline Oil Corp., Husky Energy, Shell Canada, Repsol Oil & Gas Canada Inc.

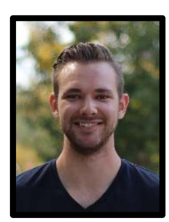

Ziguang Su

B.Eng. Exploration Geophysics, 2017, China University of Petroleum, China
B.A. English, 2017, China University of Petroleum
M.Sc. Geophysics, 2018, University of Calgary

Ron Weir

B.Sc. Geophysics, 1978, University of Alberta

- Work Experience: Harvest Operations Corp/KNOC

Lei Yang

B.Sc. Exploration Geophysics, 2015, China University of Petroleum, China

Tianze Zhang

B.Sc. Applied Geophysics, 2015, Jilin University, China
M.Sc. Geological Engineering, 2018, Jilin University, China

Kai Zhuang

B.Sc. Geophysics, 2018, University of Calgary

ASSOCIATED FACULTY and SCIENTISTS

Andreas Cordsen
Technical Advisor, CREWES, University of Calgary

M.Sc. Geology, 1975, Queen's University, Kingston
M.Sc. Geophysics, 1980, Dalhousie University, Halifax

- Work Experience: BEB, Esso Resources, Norcen Energy, GEDCO, Schlumberger, CHAD Data Ltd.

Patrick F. Daley

B.Sc. Mathematics, 1974, University of Alberta
M.Sc. Physics 1976, University of Alberta
Ph.D. Geophysics, 1979, University of Alberta

- Work Experience: Independent contractor associated with research centres of major oil companies, CREWES

Sam Gray
Technical Advisor, CREWES, University of Calgary

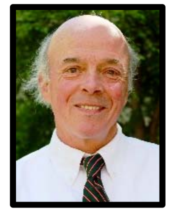

B.S. Math, 1970, Georgetown University
Ph.D. Math, 1978, University of Denver

- Work experience: U.S. Naval Research Lab, General Motors Institute, Amoco, BP, Veritas, CGG

Faranak Mahmoudian
Technical Advisor, CREWES, University of Calgary

B.Sc. Applied Physics, 2000, K. N. Toosi University of Technology, Iran
M.Sc. Geophysics, 2006, University of Calgary
Ph.D. Geophysics, 2013, University of Calgary

- Work Experience: Shell Canada, Earth Signal Processing

Claude Ribordy
Technical Advisor, CREWES, University of Calgary

Dipl. Physics, 1960, Eidgenossische Technische Hochschule ETH, Zurich
Ph. D. Nuclear Physics, University of Fribourg

- Work Experience: Aquitaine Canada, Petro-Canada, BP, Hampson-Russell Software Ltd, CGG

Brian H. Russell
Adjunct Professor, Department of Geoscience, University of Calgary

B.Sc. Physics, 1972, University of Saskatchewan
Honours Certificate in Geophysics, 1975, University of Saskatchewan
M.Sc. Geophysics, 1978, University of Durham
Ph.D. Geophysics, 2004, University of Calgary

- Work Experience: Chevron Geoscience Company, Teknica Resource Development, Veritas Software Ltd., Hampson-Russell Software Ltd, CGG GeoSoftware

Robert R. Stewart
Cullen Chair in Exploration Geophysics, University of Houston
Adjunct Professor, Department of Geoscience, University of Calgary

B.Sc. Physics and Mathematics, 1978, University of Toronto
Ph.D. Geophysics, 1983, Massachusetts Institute of Technology

- Work Experience: Veritas Software Ltd., Gennix Technology Corp., University of Calgary

Xiucheng Wei
Technical Advisor, CREWES, University of Calgary

B.Sc. Geophysics, 1982, China University of Petroleum
M.Sc. Geophysics, 1992, China University of Petroleum
Ph.D. Geophysics, 1995, China University of Petroleum

- Work Experience: China National Petroleum Company (CNPC), China University of Petroleum (CUP), British Geological Survey (BGS), China Petroleum & Chemical Corporation (Sinopec), International Research Coordinator with the Faculty of Science at the University of Calgary

Joe Wong

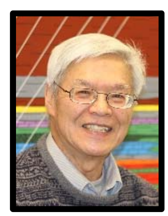

B.Sc. Physics/Mathematics, 1971, Queen’s University
M.Sc. Applied Geophysics, 1973, University of Toronto
Ph.D. Applied Geophysics, 1979, University of Toronto

- Work Experience: Ontario Ministry of the Environment, University of Toronto, JODEX Applied Geoscience Limited, CREWES

Matt Yedlin
Associate Professor, Department of Electrical and Computer Engineering, University of British Columbia

B.Sc. Honors Physics, 1971, University of Alberta
M.Sc. Physiology, 1973, University of Toronto
Ph.D. Geophysics, 1978, University of British Columbia

- Work Experience: Conoco

Student Theses

The following theses were completed with CREWES in 2018:

M.Sc.	Dennis Ellison	Depth imaging with reflection statics derived from model-based moveout
M.Sc.	Evan Mutual	Time-lapse rock physics inversion of thermal heavy oil production
Ph.D.	Jian Sun	Computational and practical developments in single- and multi-component inverse scattering series internal multiple prediction

NOTES

Evaluation of PP and PS binning for a multicomponent seismic survey from west-central Alberta

Hussain Aldhaw† and Don C. Lawton

ABSTRACT

A multicomponent seismic survey undertaken recently in west-central Alberta is evaluated for PP and PS binning methods. A 50 km^2 subset of the real survey was selected for analysis and subsequent processing. A major step in seismic processing is binning and deciding on the optimum bin size, especially for PS data. One of the common methods is ACP (Asymptotic Common Point), because it requires only an average Vp/Vs ratio and the binning is independent of the depth of the target horizon.

The simulated design is used to test for the optimum ACP binning parameters. It was designed based on the acquisition parameters of the real survey, and on the analysis made on the synthetic data set. A synthetic seismogram was created by convolving well log reflectivity data (from Vp, Vs and density logs) from a nearby well with a wavelet that represents the data. The reflection amplitudes and transmission losses are calculated using the Zoeppritz equations. Maximum useable offset was chosen based on the actual survey geometry for the depth of interest. Then it was used for the simulated survey design to evaluate the fold and offset distribution for both PP and PS datasets of the field survey.

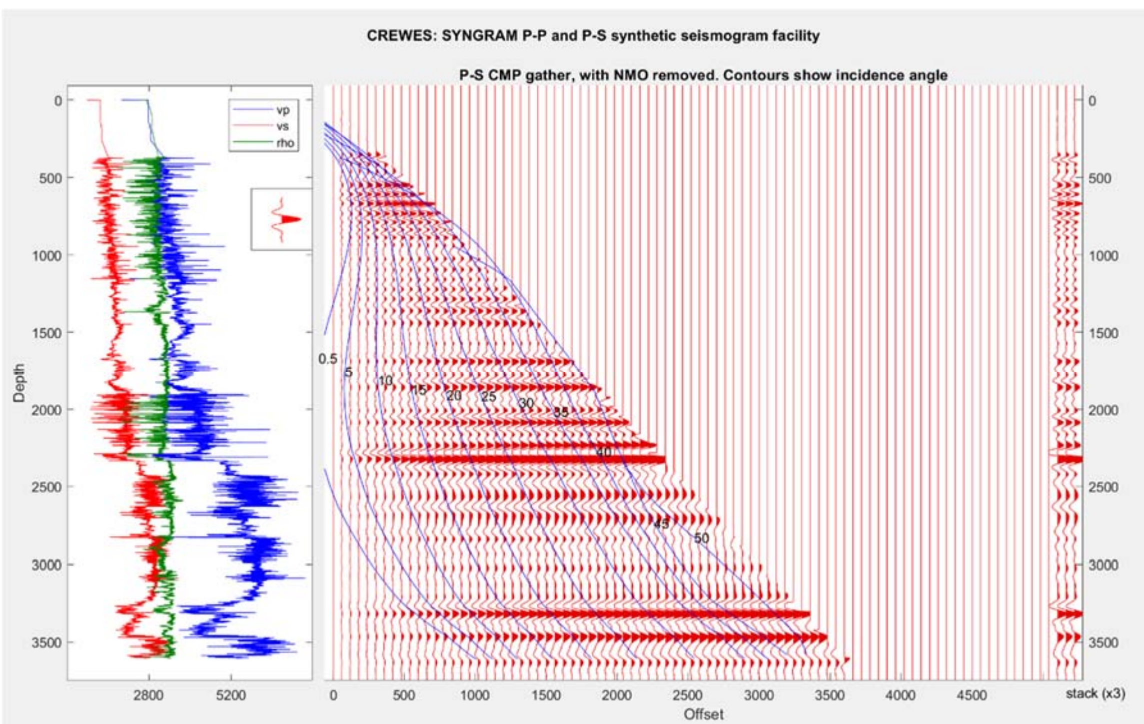

FIG. 1. PS synthetic data seismogram created using well logs from near the study area.

A brief look at CREWES fieldwork in 2018

Kevin L. Bertram[†], Kevin W. Hall, Kris Innanen, Malcolm Bertram, and Don C. Lawton

ABSTRACT

CREWES continues to use acquisition equipment to carry out surveys year round. These surveys are designed in house to gather data and test theories. It also provides an excellent opportunity for students and researchers at CREWES to witness first-hand how field data is collected. Furthermore, some researchers have actively been involved in data collection which they have then used for their reports this year.

Acquisition projects that CREWES took part in 2018 include: a) several small surveys at the CaMI Field Research Site; b) although not technically an acquisition project CREWES took part in the 2018 Earth Science for Society event; c) the 2018 Geophysics undergraduate Field School; d) a walkaway/walkaround VSP; e) the deployment and test of a multicomponent DAS layout.

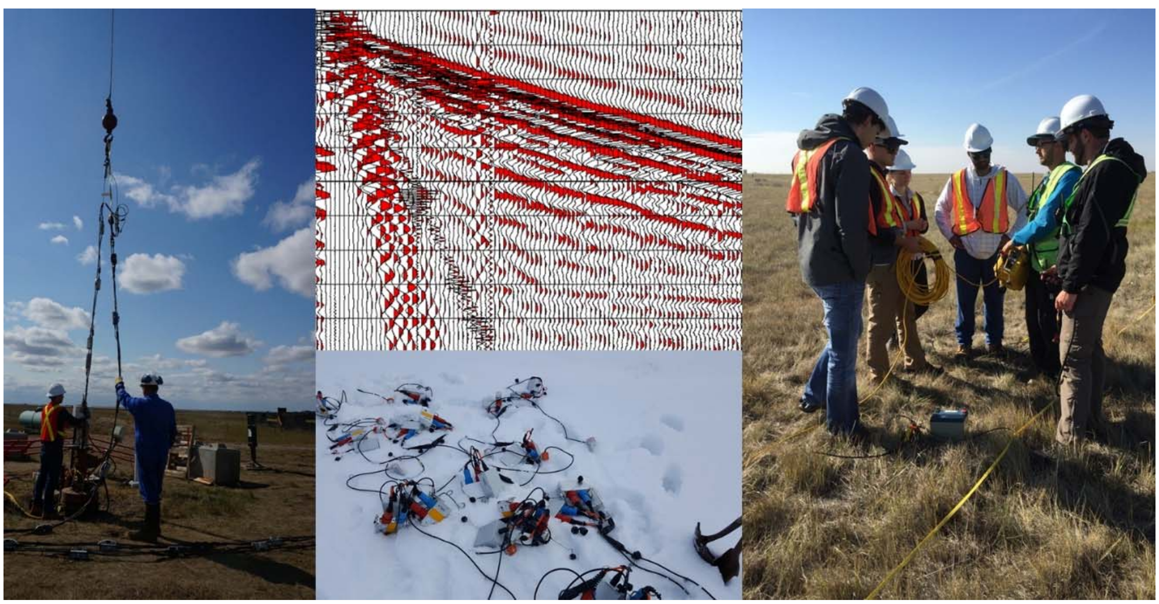

FIG. 1. Some examples of equipment being used in the field as well as a shot of raw data from the geophysics field school.

Monitoring methane gas migration in a near surface confined aquifer using electrical resistivity tomography

Timothy Cary*†, Rachel Lauer, and Kris Innanen

ABSTRACT

An 85% Methane composite gas was injected into a near surface confined aquifer at a rate of 1.5m^3 per day, for 66 days from June 12th to August 16th, 2018. The field site, located in north-eastern British Columbia, is characterized as a fluvioglacial depositional environment which is consistent with the setting of the majority of energy wells in Alberta and British Columbia, Canada. 12-m of diamitic clay seal the injection target; a 14-m thick aquifer consisting of interbedded fine-grained sands and silts. Injection was focused at the base of the aquifer at 26-m depth. Electrical resistivity tomography (ERT), combined with distributed temperature sensing (DTS), was employed to monitor the migration and fate of the gas plume during and after the injection period. Three ERT lines were permanently installed for time lapse monitoring, two parallel and one orthogonal to groundwater flow (NW-SE), centered on or close to the injection location. Dipole-dipole and gradient arrays were employed on five occasions during injection and the data combined and inverted using RES2DINV to produce time lapse difference images. Results show resistivity increases of 15-25% near the injection zone. The gas plume is interpreted as spreading laterally until buoyancy driven preferential pathways are encountered to shallower depths. Resistivity increases of 15-25% are also seen at 10-12m depth that coincide with gas flow observed at a monitoring well at 12m depth (Figure 1). DTS data were incorporated to correct the inversions for temperature effects. The general structure of the resistivity changes remains the same after temperature corrections are applied.

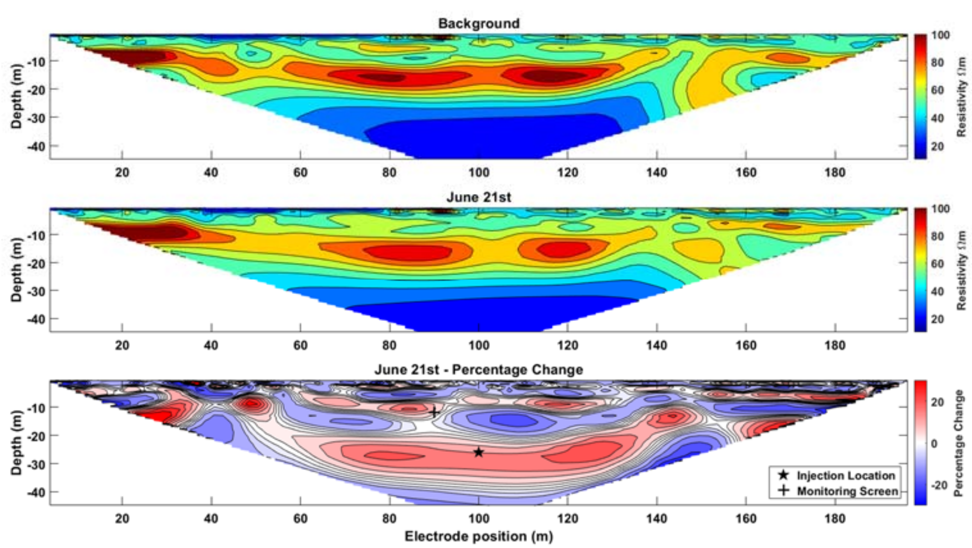

FIG. 1. Inverted resistivity models from ERT line 1 with 2.5m spacing. The percentage difference between the background survey (Top) and June 21st survey (Middle) is shown in the bottom image. The star indicates the injection point and the plus indicates a 12m deep monitoring screen where free phase gas was detected.

Estimating dry fracture weaknesses and pressure relaxation parameter in reservoirs containing aligned cracks

Huaizhen Chen*, Junxiao Li, and Kris Innanen

ABSTRACT

We derive a simplified and frequency-dependent stiffness matrix in the case that the rock contains aligned partially saturated cracks, and in the stiffness matrix we also involve the effect of pressure relaxation that is a sensitive fluid factor directly influenced by fluid viscosity and saturation. Using perturbation in stiffness matrix for an interface separating two attenuative cracked media and relationship between scattering potential and reflection coefficient, we propose a linearized reflection coefficient in the case of P-wave incidence and P-wave scattering, which is an azimuth- and frequency-dependent function of dry rock elastic property, dry fracture weaknesses and pressure relaxation related parameter. Using difference in the reflection coefficients between azimuthal angles, we derive an expression of quasi difference in elastic impedance (*QDEI*) that is mainly affected by dry fracture weaknesses and pressure relaxation related parameter. Using the derived *QDEI*, we establish an inversion approach of employing frequency-dependent differences in seismic amplitudes to estimate dry fracture weaknesses and pressure relaxation related parameter. Applying the established approach to synthetic datasets, we conclude the approach can obtain acceptable inversion results of dry fracture weaknesses and pressure relaxation related parameter in the case of generated synthetic data containing a moderate signal-to-noise ratio (SNR). Test on a real data set reveals that the inversion results of dry fracture weaknesses provide a reliable tool in fracture prediction, and the estimated pressure relaxation related parameter appear as an additional proof for the discrimination of fluids in cracks.

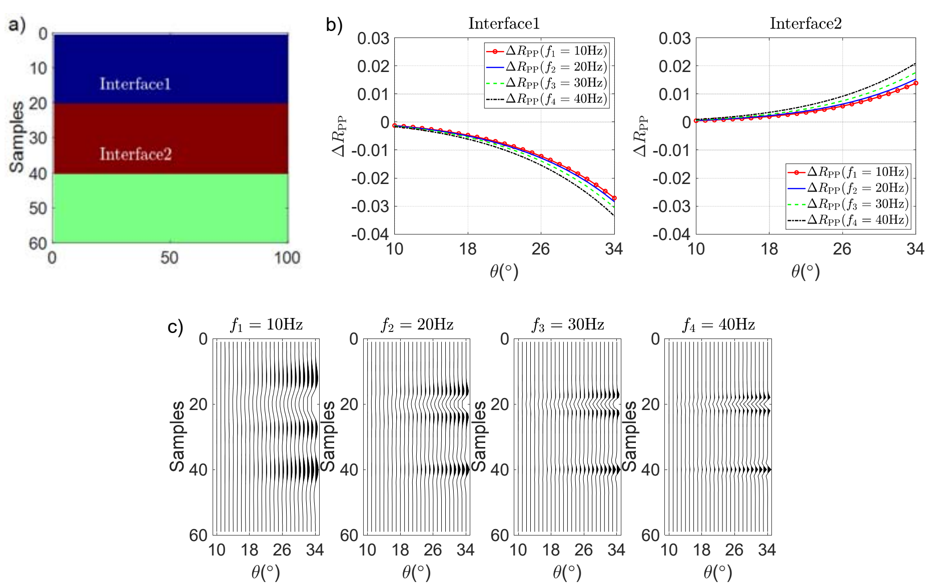

FIG. 1. a) Three-layer model; b) Comparisons between reflection coefficient differences of different frequencies; and c) Comparisons between seismic amplitude differences of different frequencies.

Inversion of azimuthal seismic amplitude differences for tilted fracture weaknesses

Huaizhen Chen† and Kris Innanen

ABSTRACT

Based on the linear slip fracture model, we first express the stiffness matrix of tilted transversely isotropic (TTI) media in terms of the normal and tangential fracture weaknesses. Using perturbations in stiffness parameters for the case of an interface separating an isotropic medium and a TTI medium, we derive a linearized P-to-P reflection coefficient as a function of fracture weaknesses, in which titled fracture weaknesses involving effects of tilt angle and fracture weaknesses emerge. Following a Bayesian framework, we propose an inversion approach to use amplitude differences between seismic data along two azimuths to estimate the tangential fracture weakness and tilted normal and tangential fracture weaknesses based on the derived and simplified reflection coefficient. Synthetic tests confirm that the unknown parameter vector involving the tangential fracture weakness and tilted fracture weaknesses is estimated stably and reliably in the case of seismic data containing a moderate Gaussian noise. The inversion approach is also applied to a field data set acquired from a fractured carbonate reservoir, from which reasonable results of tilted fracture weaknesses are obtained. We conclude that the proposed inversion approach may provide additional proofs for fracture characterization, and it also make the estimation of tilt angle from observed seismic data for fractured reservoirs be available.

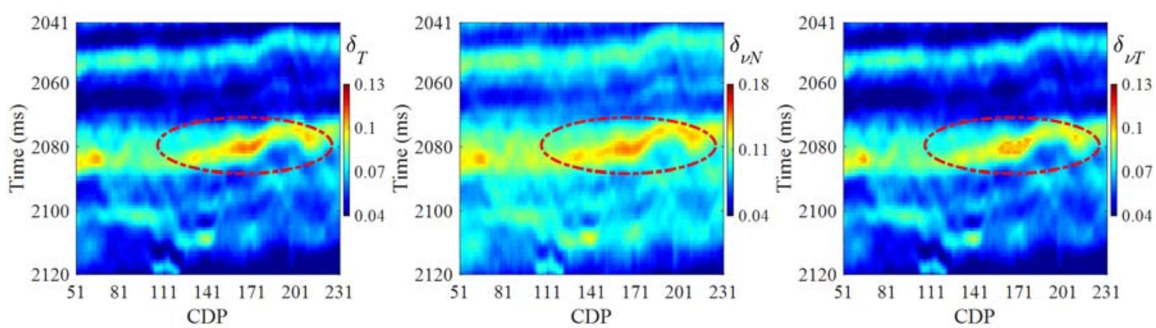

FIG. 1. Inversion results of tangential fracture weakness δ_T and titled normal and tangential fracture weaknesses $\delta_{\nu N}$ and $\delta_{\nu T}$.

Nonlinear inversion for effective stress sensitive parameter using observed seismic data

Huaizhen Chen, Junxiao Li, and Kris Innanen

ABSTRACT

Estimation of effective stress has become an important task in reservoir characterization and can guide the selection of fracturing area in unconventional hydrocarbon reservoirs. Based on Gassmann's fluid substitution model, we propose a workflow of employing observed seismic data to implement nonlinear inversion for dry rock moduli, fluid factor and stress-sensitive parameter. We first make an approximation of fluid substitution equation, in which we replace the porosity term with a stress-sensitive parameter. Using stiffness parameters related to the stress-sensitive parameter, we derive a linearized reflection coefficient as a function of reflectivity of stress-sensitive parameter, and we also transfer the reflection coefficient to elastic impedance (EI). The proposed workflow involves estimating EI datasets from seismic data stacked over different ranges of incidence angle and utilizing the estimated EI to implement the inversion for the stress-sensitive parameter. We stress that a model-based least-squares inversion algorithm is used to implement the estimation of EI and a nonlinear inversion approach is employed to estimate the unknown variables from the estimated EI, which is implemented as a four-step inversion. Synthetic data generated using Zoeppritz equation are utilized to verify the stability of the proposed approach. A test on a real data set acquired over a gas-bearing reservoir reveals that the propose workflow appears to preserve as a useful tool to provide reliable results for fluid identification and stress prediction.

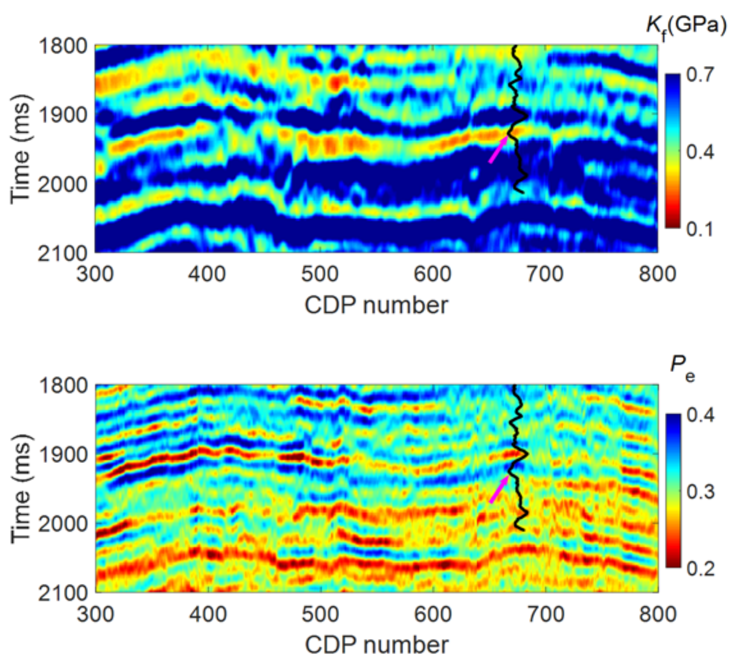

FIG. 1. Inversion results of fluid factor and stress-sensitive parameter.

DAS applications for near-surface characterization and traffic conditions assessment

Raúl Cova†, Heather K. Hardeman-Vooys, Da Li, and Matt McDonald

ABSTRACT

Using distributed acoustic sensing (DAS), previously deployed telecommunication optical fibres can be repurposed as permanent seismic sensors. The ability of this system to acquire data for large distances (>10 km) and with a dense sampling (<1 m) makes this technology very attractive for near-surface monitoring and characterization. We show two applications that illustrate the potential of DAS data for these purposes. First, by using interferometric principles, we compute virtual source gathers from the ambient noise recorded by the fibre. This process allowed us to reconstruct the surface-wave propagation that would have been recorded between two different points along the fibre simulating an active source experiment. Then, dispersion spectra were computed from the data showing the ability of the DAS data to provide the necessary input for near-surface characterization methods like MASW (multichannel analysis of surface waves). A second application of DAS is explored using data acquired along the C-train tracks in the City of Calgary. From the raw data, it is possible to identify the signature of different sources propagating with different apparent velocities. Here, we compute the velocities of these signals by using trace-by-trace crosscorrelations. Assuming that most of these signals are generated by vehicles driving along the roads next to the C-train tracks, this information can be used for monitoring traffic condition in terms of the velocity of the vehicles recorded at any time of the day. We also compute spatial average velocities that can be used to interpret changes in traffic conditions throughout the day in a given section of the road.

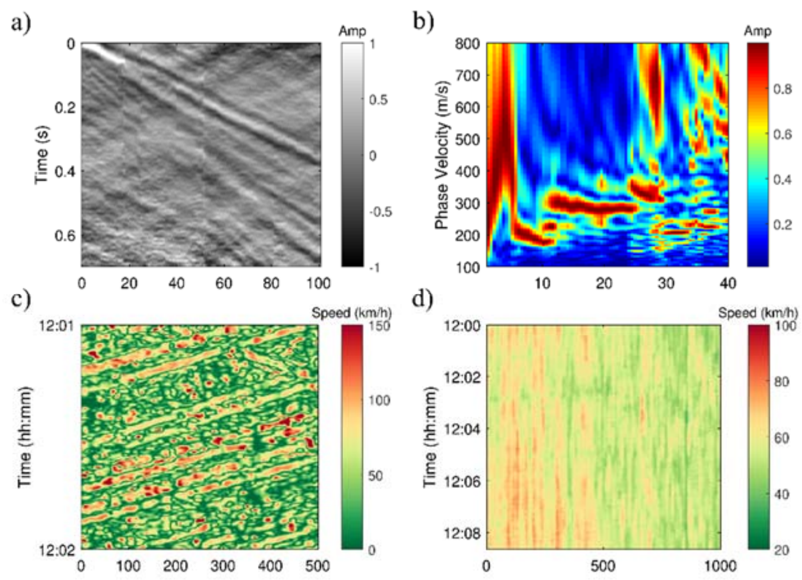

FIG. 1. (a) Virtual source gather computed using ambient noise recorded with an optical fibre. (b) Dispersion spectrum of the data in (a). (c) Instantaneous velocities of the signals propagating in a 1-minute window over 500 m of the optical fibre deployed along the C-train tracks. (d) Average velocities for a period of 10 minutes for a 1 km section along the C-train tracks.

Pre-conditioning walkaway VSP data for elastic FWI

Raúl Cova*, Kris Innanen, and Marianne Rauch-Davies

ABSTRACT

Full waveform inversion (FWI) applications on land seismic data remain very limited. The presence of strong anelastic effects, near-surface heterogeneities, unknown source and receiver signature and poor signal-to-noise ratio, among other reasons, challenge the capabilities of most modelling and inversion algorithms. Here, we perform an elastic FWI using land VSP data acquired in a walkaway configuration. We pre-process the data with the intent of improving the signal-to-noise ratio and removing undesired effects. Elevation differences among source locations were accounted for by applying elevation static corrections. Signal-to-noise ratio was improved by using a predictive filter in the FX domain. Two datasets with different deconvolution conditions were generated. A deterministic deconvolution using the recorded downgoing wavefield was applied to one of the datasets to remove the source signature. Even though this process partially accounts for changes in the wavelet with depth, a single operator is used for all the events recorded on a given trace. For this reason, we also computed a Gabor deconvolution to account for non-stationarity in the source signature. Then, we performed an elastic FWI using a multiscale approach, with four frequency bands (4-8 Hz, 4-12 Hz, 4-16 Hz and 4-20 Hz) and three different depth windows (250-1000 m, 750-2250 m and 2000-3500 m). The FWI performed on the data deconvolved with the deterministic operators converged toward a solution that was closer to the sonic logs available in the well. Despite providing a wider frequency spectrum, the FWI using the Gabor deconvolved data did not converge toward an optimal solution. A closer examination of the input data revealed that in addition to removing some of the multiples, the deterministic deconvolution resurfaced some downgoing S-wave events that were not evident before. Providing data with less complexity and enhancing prominent events provided us with a more robust initialization of the inversion problem.

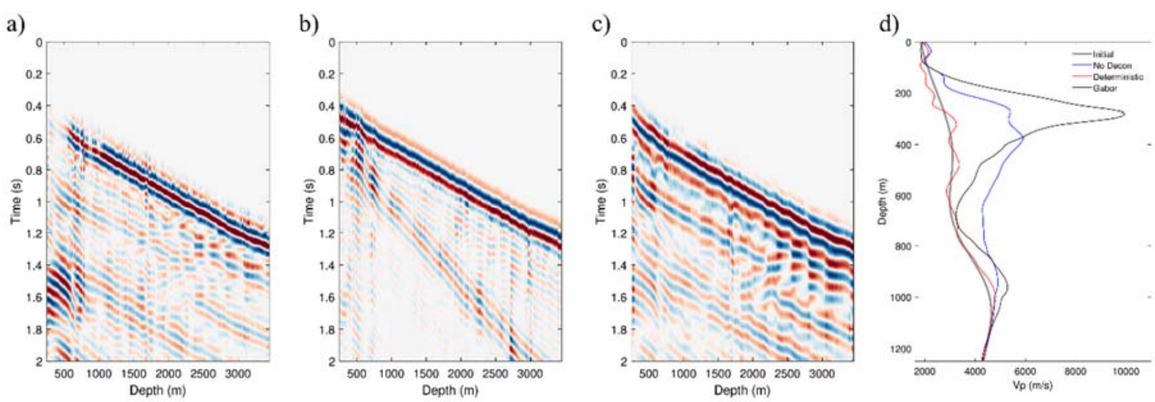

FIG. 1. Pre-processed data filtered at the band of the initial scale (4-8 Hz). (a) Data without deconvolution. (b) Deterministic deconvolution output. (c) Gabor deconvolution output. (d) FWI results for the first depth window. The Gabor and non-deconvolved data diverge significantly from the initial model. However, the data deconvolved using deterministic operators is stable and is starting to add more details around the initial model.

Frequency domain adaptive waveform inversion

Matt Eaid†, Scott Keating, and Kris Innanen

ABSTRACT

Full waveform inversion (FWI) attempts to find a high-resolution model of subsurface parameters carrying a high likelihood of having produced the observed seismic data. While classic FWI is generally quite successful, the extreme nonlinearity involved in seismic inverse problems, coupled with the oscillatory nature of seismic data, can invoke a phenomenon known as cycle skipping, leading to locally minimized objective functions. Generally, when cycle skipping occurs the updated model is a worse representation of the true subsurface than the starting model was.

Extended waveform inversion is a relatively new idea that is an umbrella for a suite of inversion techniques that extend the model space, usually by some nonphysical parameter, and then drive that parameter to an ideal quantity, matching the predicted to the observed data. They combat the cycle skipping problem by adding a degree of freedom to the model space and forming objective functions that do not rely on sample-by-sample differences. The flavour of extended waveform inversion we present is known as adaptive waveform inversion (AWI) which extends the model space in convolutional Wiener filter coefficients and attempts to drive them towards a zero-lag delta spike. Originally derived in the time domain, we present a frequency domain alternative and discuss special considerations for frequency domain implementation. We then show one example where AWI is more robust then FWI and discuss the challenges going forward.

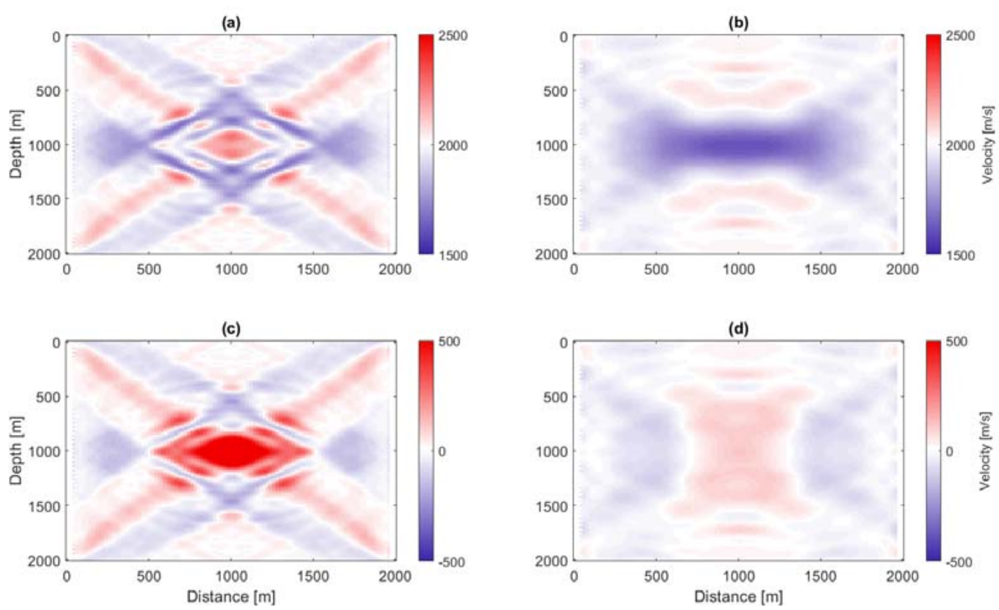

FIG. 1. Inversion results for steepest descent optimization, from a model that induces cycle skipping. The inversion was computed over one frequency band from 3-20Hz for 25 iterations. (a) Velocity model recovered by FWI, (b) velocity model recovered by AWI, (c) difference between true Gaussian anomaly and the FWI inverted model, (d) difference between the true Gaussian anomaly and the AWI inverted model.

Toward 4C FWI: DAS and 3C as complementary datasets

Matt Eaid*, and Kris Innanen

ABSTRACT

Full waveform inversion (FWI) is a useful, and powerful tool for finding accurate estimates of the subsurface parameters. However, when applied to conventional land data, the quality of the inversion result can suffer from nonideal acquisition. FWI is most successful when we have densely sampled, wide aperture data, with a large bandwidth. Seismic data acquired with standard three component (3C) geophones typically lacks the low frequencies and dense sampling required for successful inversions. Recent advances in the use of distributed acoustic sensors (DAS) may hold the key to remediation of these problems. Distributed acoustic sensors employ a continuous optical fibre, offering tighter spatial sampling at a greatly reduced cost, especially in the borehole environment. It has also been shown in laboratory experiments, that DAS fibres can recover significantly lower frequencies than standard 3C geophones. The trade-off is that DAS fibres only sense strain along their tangent and therefore only provide us with one component, at a lower signal-to-noise ratio, limiting our ability to invert for elastic parameters. Taken together, both datasets share complementary aspects that should benefit FWI.

In September of 2018, CREWES in partnership with the Containment and Monitoring Institute (CaMI), acquired a large 3D walkaway-walkaround VSP dataset into both straight fibre, helical fibre, and 3C geophones in our geophysics well. Future work will focus on utilization of this dataset to develop an FWI formulation that leverages the complementary aspects of the DAS and geophone data. This paper is concerned with exploring the modelling of these complementary aspects as they relate to FWI, using the CaMI field site as our model.

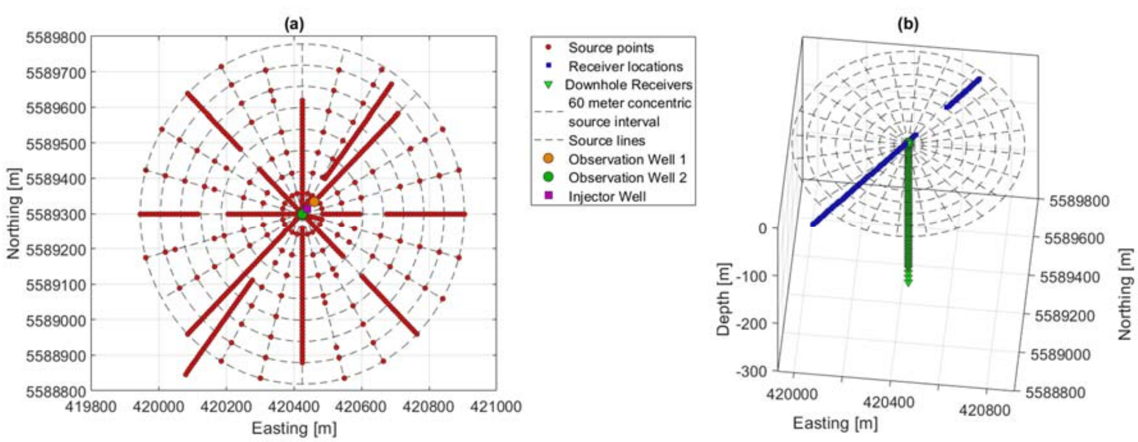

FIG. 1. (a) Plan view source geometry for 3D walkaway-walkaround vertical seismic profile acquired with straight and helical DAS fibre, and 3C geophones in Observation well 2 (green circle). (b) Receiver geometry on same grid as source geometry, surface 3C geophones shown in blue squares, and downhole 3C geophones by the green triangles. Observation well 2 also contains a straight fibre, and a helical fibre with a radius of 1 centimetre and a pitch of 30 degrees.

Viscoacoustic reverse time migration in tilted TI media with attenuation compensation

Ali Fathalian† and Kris Innanen

ABSTRACT

Simulation of wave propagation in an anisotropic viscoacoustic medium is an important problem, for instance within Q-compensated reverse-time migration. Processes of attenuation, dispersion, and anisotropic influence all aspects of seismic wave propagation, degrading resolution of migrated images. We present a new approach of the viscoacoustic wave equation in the time domain to explicitly separate amplitude attenuation with phase dispersion and develop a theory of viscoacoustic reverse time migration (Q-RTM) in tilted TI media. Because of this separation, we would be able to compensate the amplitude loss effect, the phase dispersion effect, or both effects. In the Q-RTM implementation, the attenuation-compensated operator was constructed by reversing the sign of amplitude attenuation. We validate and examine the response of this approach by using it within a reverse time migration scheme adjusted to compensate for attenuation. The amplitude loss in the wavefield at the source and receivers due to attenuation can be recovered by applying compensation operators on the measured receiver wavefield.

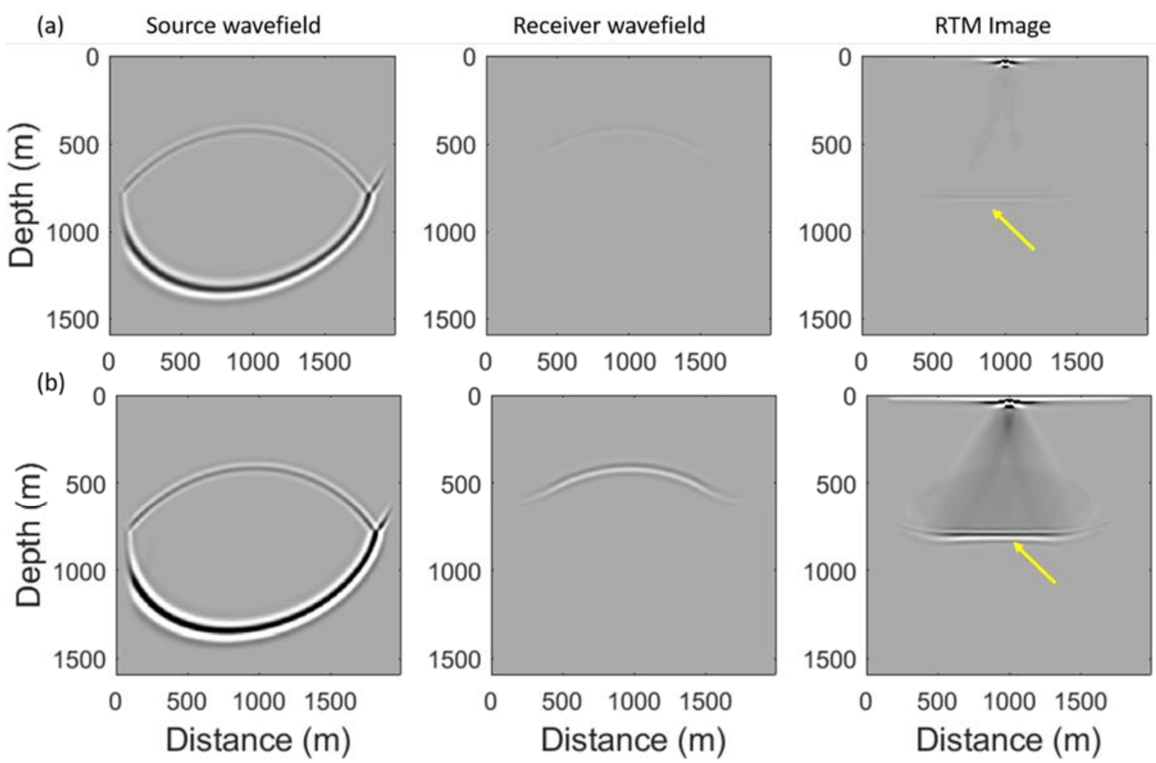

FIG. 1. Snapshots of the source wavefield, the receiver wavefield, and the RTM image at 0.5, 0.62, and 0.79 s. The viscoacoustic data are extrapolated for the receiver wavefield. Row (a) and (b) show the non-compensated and compensated snapshots respectively.

Walk away VSP processing of DAS and geophone data at the CaMI Field Research Station, Newell County, Alberta

Adriana Gordon*† and Don C. Lawton

ABSTRACT

As part of the FRS baseline assessment, several Vertical Seismic Profiles were acquired with the intention of testing emerging monitoring techniques such as Distributed Acoustic Sensing (DAS). In this report, we describe the processing flow and discuss the results obtained for a walkaway VSP oriented North-South and centred in the observation well 2. This survey was acquired in July 2017 using two recording systems: fibre optic cables (straight and helical wound fibre) for DAS and a 3C 24-level geophone array. Each section of the report displays a comparison between the straight and helical fibre optic cables and the geophone array. After processing the different datasets, we compared the results of the VSP-CDP transforms with an inline section from a 3D seismic survey crossing through the well (Figure 1). In the three cases, there is a good correlation between the events in the surface seismic and the VSP-CDP. The injection target located at approximately 250 ms is noticeable. Nevertheless, there is an apparent discontinuity of the event of interest across the mapped result, particularly for the straight fibre. The DAS datasets yield a better illumination in the shallow section due to the full coverage of the fibre in the well.

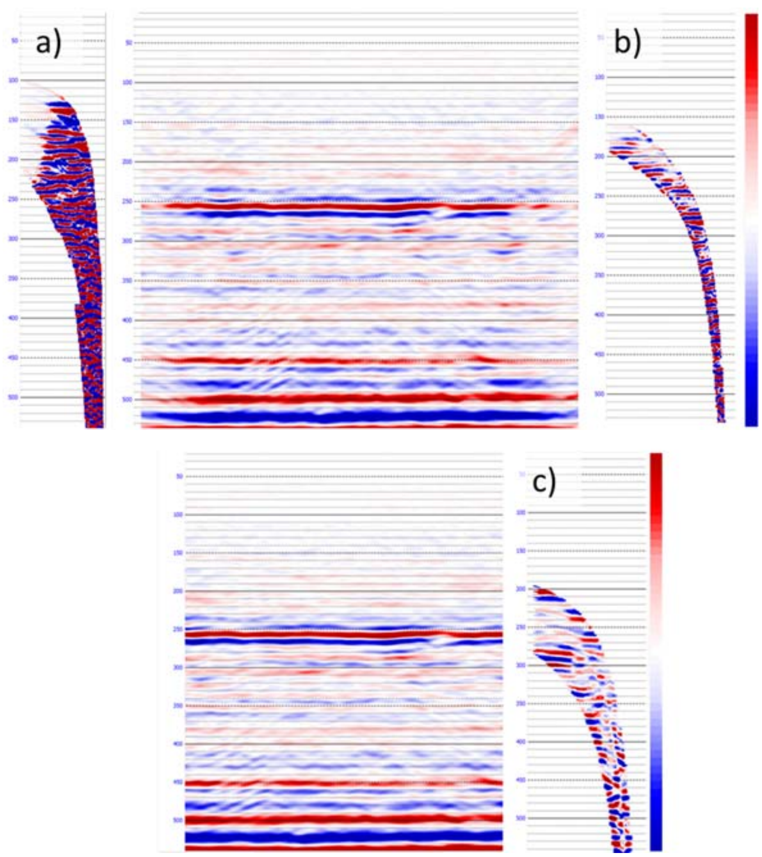

FIG 1. VSP-CDP transform of walk away VSP compared with a seismic line at observation well 2 location. a) Straight fibre VSP-CDP, b) Helical fibre VSP-CDP, c) geophone VSP-CDP transform.

Machine learning in geoscience: facies classification with features engineering, clustering, and gradient boosting trees

Marcelo Guarido*†

ABSTRACT

Facies classification is the process to determine the local rocks lithology by analyzing indirect measurements, such as well logs. Usually it is done manually by an interpreter. In this work, I am presenting an automatic method for facies classification by the use of feature engineering and gradient boosting trees. I used a set of classified well logs to train a multi-class machine learning model and compared the predictions with both raw and processed features in a blind well. I could demonstrate that preparing the, by creating new features from the original well logs, such as their gradients, polar coordinates transformations, and clustering analysis, increased the predictions accuracy from 47% to 60%.

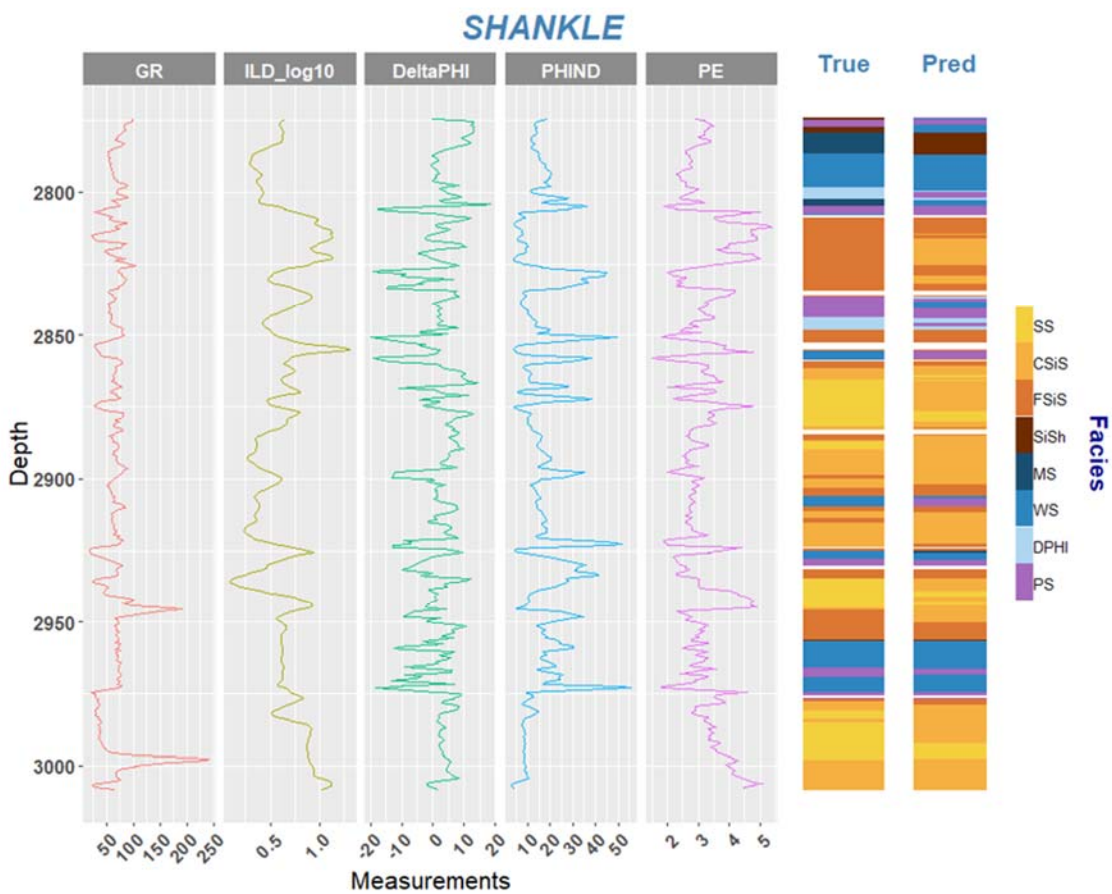

FIG. 1. Tuned predictions on the blind/evaluate well after data processing.

Machine learning in geoscience: using deep learning to solve the TGS Salt Identification challenge

Marcelo Guarido*†, Junxiao Li, and Raúl Cova

ABSTRACT

Deep learning, or neural networks, contain a widely range of applicability, that goes from regression of business analyses to treats identification on medical images. In this paper, we successfully applied a U-net based image semantic segmentation to identify salt bodies using only seismic images from the *TGS Salt Identification Challenge*. The process is simple applied with moderate computer requirement for a small set of images, but it can grow exponentially as more images are included. In the end, we could train a model that gives a 0.8 score on the *IoU* metric.

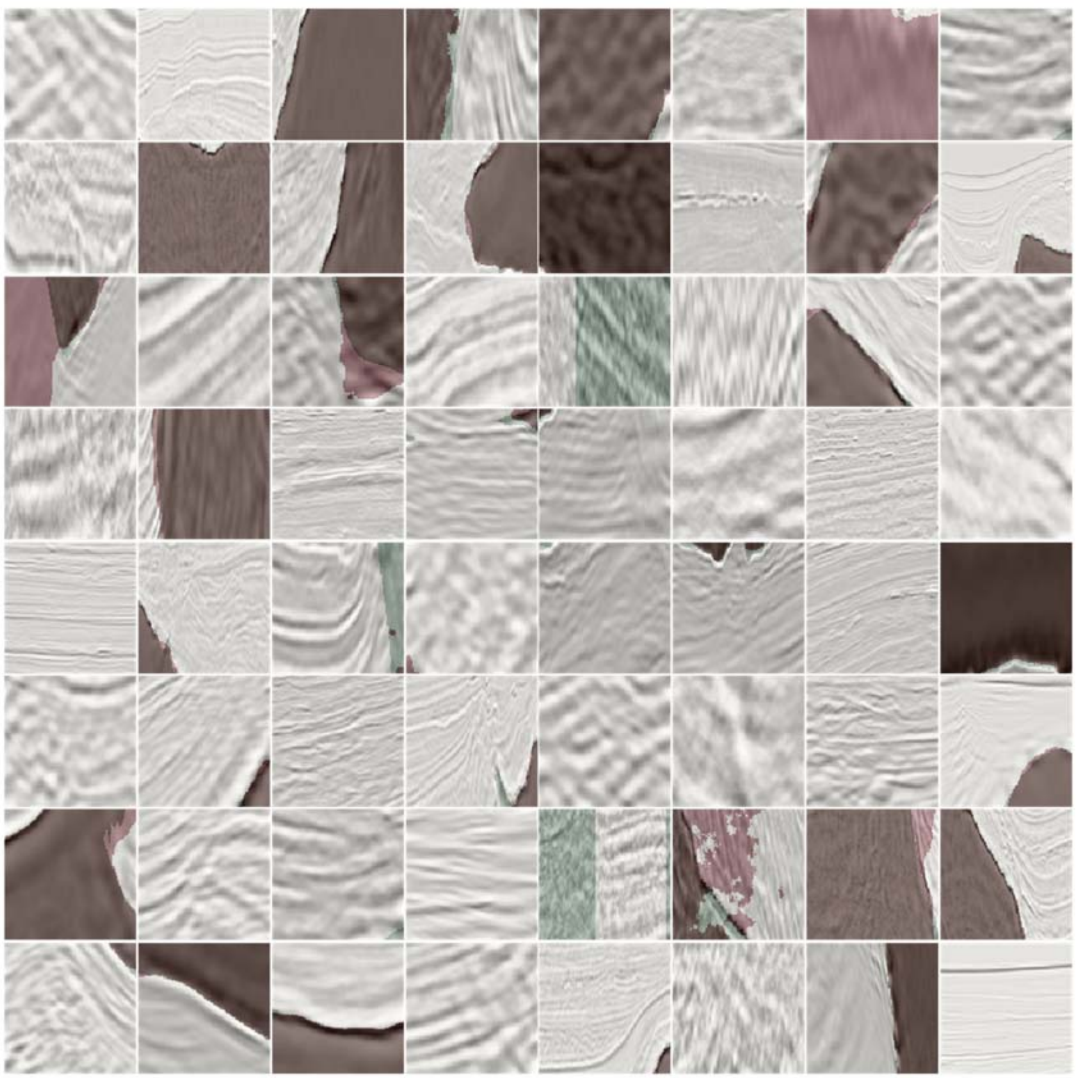

FIG. 1. Seismic overlapped by the original masks in green, predictions in red, and intersection in brown.

Upgrades to the physical modelling lab and upcoming experiments

Marcelo Guarido, Nasser Kazemi, Joe Wong, Nadine Igonin*, Kevin L. Bertram, Kris Innanen, and Roman Shor

ABSTRACT

Physical modelling has been used extensively over the history of CREWES in order to study interesting phenomena and test novel algorithms. In this report, we present updates to the physical modelling laboratory that will allow for more sophisticated experiments and increase efficiency in acquisition. New sources (both P- and S-wave) of various sizes have been purchased, as well as more digitizers that would allow for 24-channel acquisition. Additionally, the source is being upgraded in order to be able to generate complex waveforms that may be more useful for various applications. A seismic while drilling (SWD) experiment is proposed in order to test the capability of SWD signals to enhance subsurface illumination. Using a model with inherent illumination problems, synthetic tests were carried out and used to build up the model to be used in the experiment (Figure 1). Microseismic data geometry is similar to SWD, and the experiment can be repeated, but with a different source pulse for the microseismic events. Preliminary results testing the radiation pattern of various sources is presented, as well as a list of future work that includes elastic physical modelling for SWD, microseismic, and time reversal imaging.

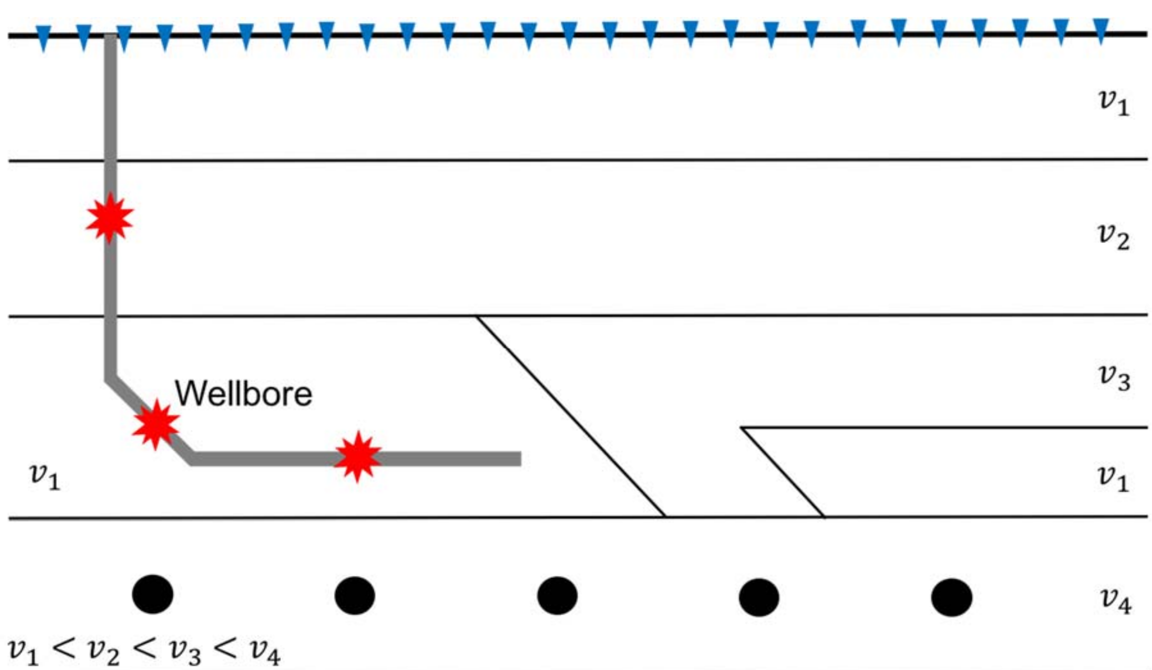

FIG. 1. Cross section of the model in construction, with receivers on the surface and sources to be embedded in the model itself.

CREWES 2018 multi-azimuth walk-away VSP field experiment

Kevin W. Hall*, Kevin L. Bertram, Malcolm Bertram, Kris Innanen, Don C. Lawton

ABSTRACT

CREWES conducted a high-resolution multi-azimuth walk-away three-component vertical seismic profile (VSP) survey at the Containment and Monitoring Institutes Field Research Station (FRS) in the first week of September 2018. This data is primarily intended for use in full-waveform inversion (FWI) and modelling studies. The FRS has three wells, referred to here (from SW to NE) as the geophysics, injection and geochemistry wells. Figure 1a shows vibe points (VP) as red dots for thirteen source lines centered on the geophysics well (observation well 2). Four of the source lines were acquired with a 10 m VP spacing (bearings 0^0, 45^0, 90^0, 135^0), and the remainder were acquired at 60 m VP spacing. The source was an Inova Univib running a linear 1-150 Hz sweep. In addition to existing permanent 3C geophones and fibre at the FRS, High Definition Seismic Corporation deployed a string of Inova 3C VectorSeis accelerometers in the geophysics well at a nominal 1 m spacing, from the surface to 324 m depth. The data are currently undergoing zero-offset and far-offset VSP processing. Figure 1b shows a zero-offset accelerometer corridor stack deconvolved with the down-going P-wavefield, compared to a P-P synthetic seismogram constructed using sonic and density well logs recorded in the geophysics well and the sweep used for VSP acquisition. First-break picks sorted by offset and azimuth appear to confirm the presence of weak anisotropy at the FRS, as observed on a single offset semi-circular walk-around VSP recorded in the injection well in 2015.

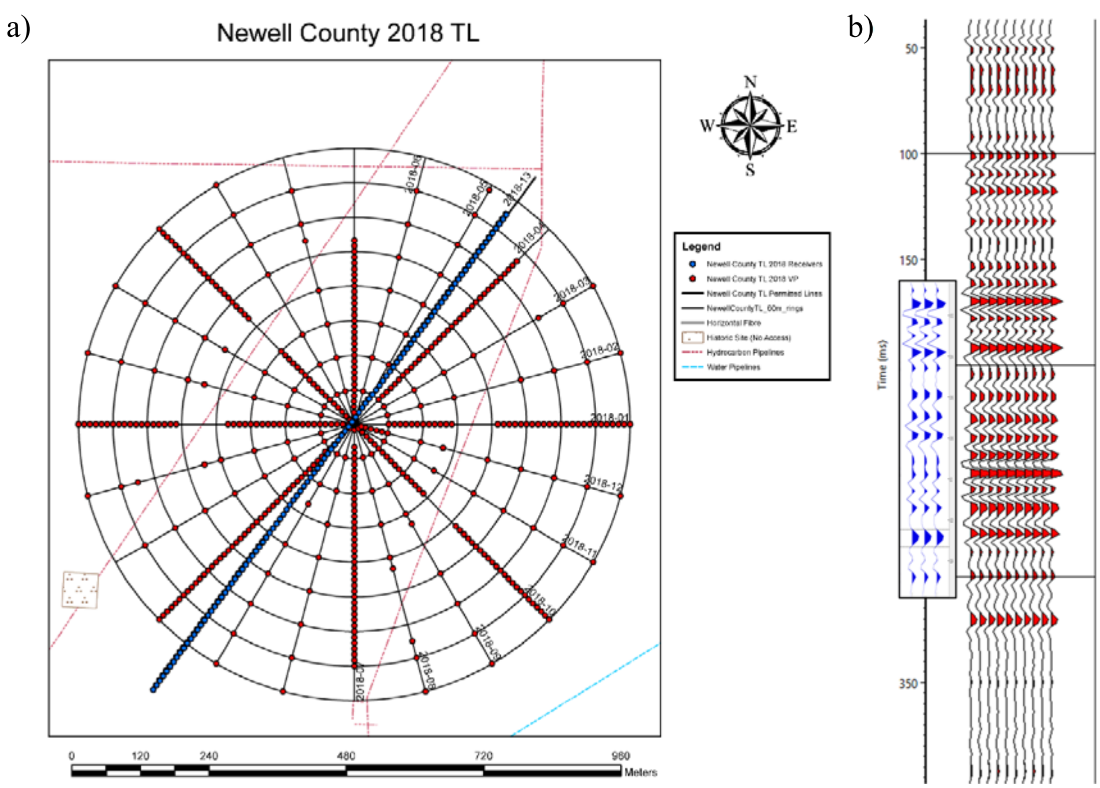

FIG.1. (a) Survey map and (b) zero-offset corridor stack (red) and synthetic seismogram (blue).

Optical fibre data registration

Kevin W. Hall[†], Don C. Lawton

ABSTRACT

The Containment and Monitoring Institute (CaMI) Field Research Site (FRS) has three wells on the lease, referred to (from SW-NE) as the geophysics, injection and geochemistry wells. Borehole and trenched optical fibres are connected in a continuous loop of ~5 km length in the following order: 1) helical fibre in geophysics well, 2) straight fibre in geophysics well, 3) straight fibre in geochemistry well, 4) straight fibre from geophysics well to south end of trench, 5) helical fibre for entire length of trench and 6) straight fibre from the north end of the trench back to the geophysics well. Since we know the trace spacing for each survey, we can assign coordinates to traces once we know the position of any given trace. Tap tests in above ground junction boxes can be spread over as many as 100 traces due to gauge length effects and are not precise enough for this purpose. High-amplitude noise observed at above ground junction boxes also spreads across variable numbers of data traces, depending upon source distance from the junction box. Separation of continuous loop data into discrete datasets has been performed by running a modified STA/LTA algorithm on the sum of the squares of uncorrelated trace amplitudes to locate the edges of junction box noise, which also gives us a starting point for determining trace locations in the wells and trench. Figure 1 shows a correlated record with 0.75 m trace spacing muted using STA/LTA results for all source gathers in this example.

For borehole registration we have calculated least-squares hyperbolic fits to first-break picks to determine which is the deepest trace in each well. Tests of this process give a result with a standard deviation of one trace for straight fibre and three traces for helical fibre for a survey acquired with 0.25 m trace spacing and 10 m gauge length.

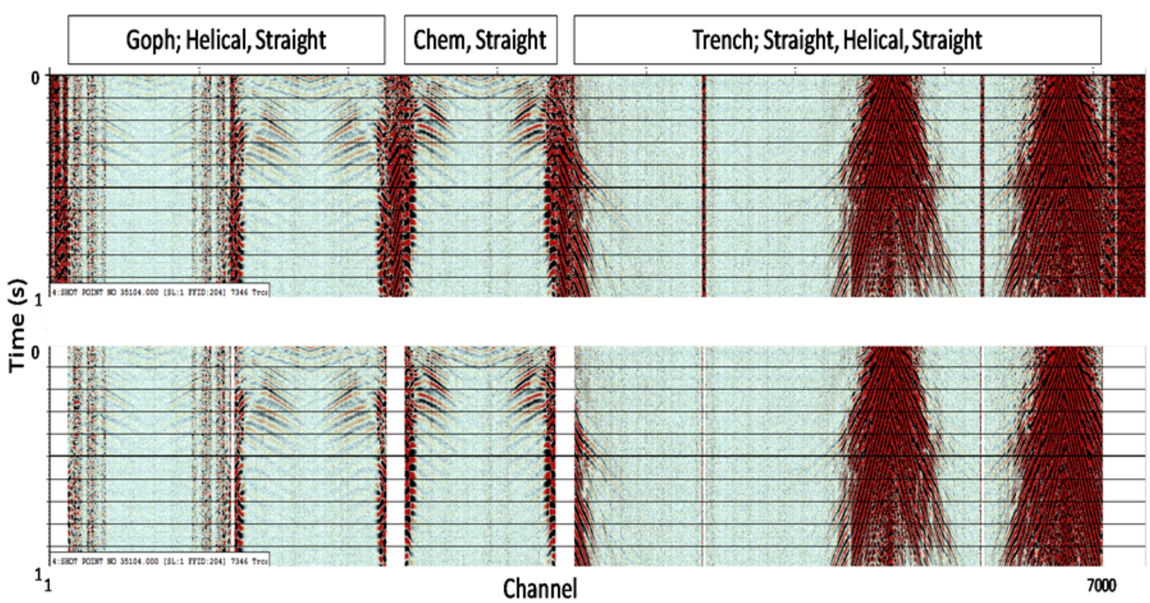

FIG. 1. Correlated data with junction box noise trace mutes calculated using a modified STA/LTA algorithm.

Analytic models of distributed acoustic sensing data for straight and helical fibre

Heather K. Hardeman-Vooys†, and Michael P. Lamoureux

ABSTRACT

We discuss the process of acquiring seismic data using distributed acoustic sensing. We then describe the analytic model used to depict this process. We find the strain tensor for the full-waveform by separating the problem in to the case for the P-wave strain tensor and the S-wave strain tensor. We show examples of the model for the P-wave response of the fibre in two different media. We compare the results of the S-wave response for helical and straight fibre. Finally, we examine the full-waveform response of the fibre and consider the results using different gauge lengths.

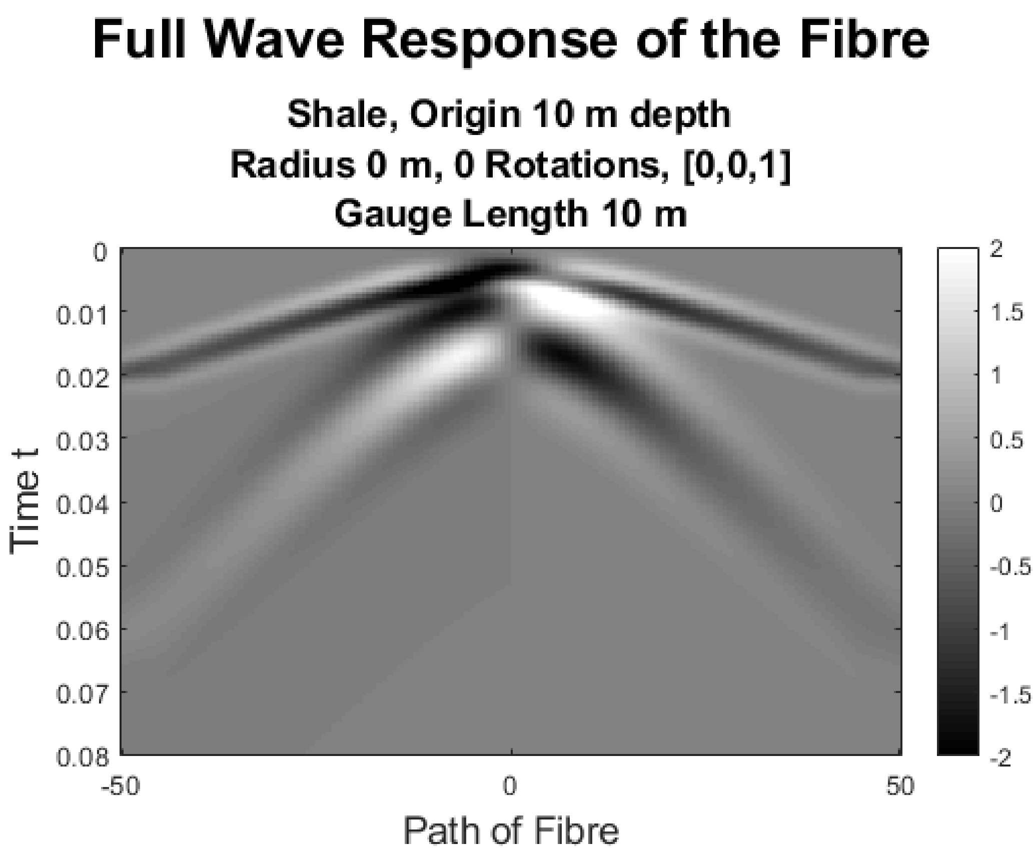

FIG. 1. The full-waveform response of the straight fibre in saturated shales when the gauge length is set to 10 m.

VSP using distributed acoustic sensing at the CaMI Field Research Station in Newell County, AB – August 2018

Heather K. Hardeman-Vooys*, Matt McDonald, and Michael P. Lamoureux

ABSTRACT

We examine the seismic data acquired by Fotech at the the Containment and Monitoring Institute Field Research Station (CaMI FRS) in Newell County, AB in August 2018 using distributed acoustic sensing. We describe the schematic of the fibre at CaMI FRS and explain the experiment. We then show the results of various aspects of the experiment focusing on the vertical seismic profiling of the straight fibre in the two wells at the site.

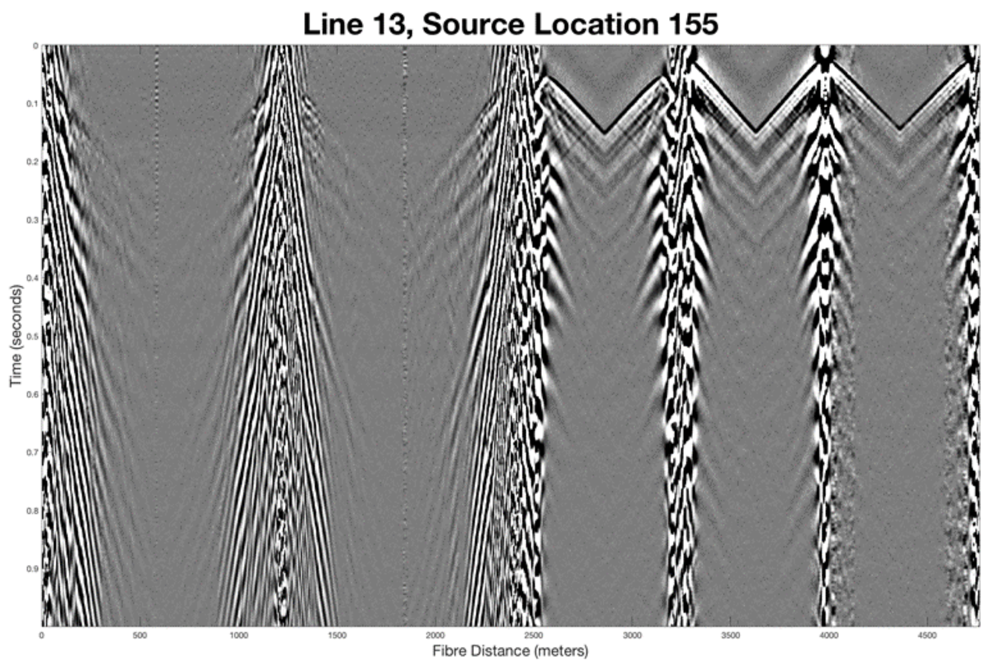

FIG. 1. DAS data acquired by Fotech at the CaMI FRS site in Newell County, AB when the vibroseis truck was at source location 155. The left portion of the image shows the beginning of the trench with the source located in the middle of the trench. After the trench, the straight fibre from well 1 can be seen which is followed by the straight fibre in well 2 and then the helical fibre in well 2.

Getting it right: source-receiver offsets in the radial trace transform

David C. Henley†

ABSTRACT

Our original radial trace (RT) transform was only intended to be applied to 2D source/receiver ensembles, for which source-receiver offset values are almost always linearly distributed. Hence, when we implemented the inverse RT transform we adopted an approximation: the source-receiver offset values used in the inverse transform to populate the trace headers of the output X/T ensemble are interpolated from the values of XMIN and XMAX placed in the radial trace headers by the forward transform. Eventually, however, we needed to apply the RT transform to 3D receiver line ensembles. Here, the linear offset approximation is no longer accurate, since the offset distribution is hyperbolic when the source position is not collinear with the receiver line. This distorts the mapping of data values into the X/T domain during the inverse RT transform, the distortion increasing with the distance of the source from the line. This is not an issue for the stand-alone radial trace filter, in which the forward/inverse R/T transform is internal to the module, and thus always has access to trace headers from the X/T input; but we encounter the problem for any process in which RT domain data are processed externally as RT traces and subsequently inverted to an X/T ensemble.

We have updated our RT transform module for SeisSpace so that it now offers the option of restoring original X/T offset values to the headers of the inverse transform, in addition to the other original offset interpolation options, implemented primarily as diagnostics. We document the changes here, describe the steps necessary in order to use the updated module, and show examples of the new module applied to 2D data with source positions displaced from the line. We also review the original 2D offset interpolation options still available in the current version of the inverse transform.

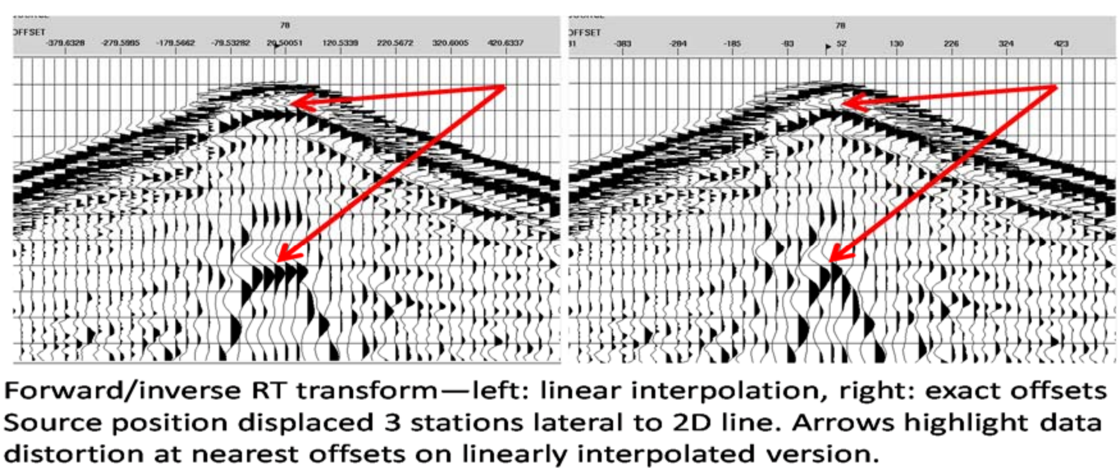

FIG. 1. Zoom view of a source gather with source displaced 3 stations laterally from the line. Left: Linear offset interpolation used in the RT inverse transform causes distortion of data at the nearest offset values. Right: When correct offset values are used during the inverse RT transform, no such distortion appears.

Seismic Oil of Olay: wrinkle reduction on 3D source ensembles

David C. Henley*

ABSTRACT

We have shown in other work that interferometric principles can be used to remove effects of the irregular near-surface layers from seismic reflection data. Our method, raypath interferometry, has been successfully applied to several 2D seismic lines, and has proven comparable or superior to conventional surface correction methods, particularly for converted wave data, or for any dataset where surface-consistency is not satisfied, and non-stationary surface correction is required. It has also been demonstrated that raypath interferometry can be applied to small 3D seismic surveys, but that the processing burden makes the full 3D method unattractive for larger surveys. We explore here alternative methods that still employ some of the methodology of the complete procedure.

We show here the results of experimental pre-processing, based on interferometric principles, applied to large 3D source gathers, in which we attempt to remove, at least partially, the near-surface effects at the receivers within a 3D array, independently for each shot. We envision this as the first step of a two-part process, in which the second step subsequently removes near-surface effects between source locations prior to CMP stacking or imaging. We demonstrate three interferometric approaches to removing near-surface effects from receiver locations within source ensembles. Just as the application of Oil of Olay attempts to reduce facial wrinkles on mature adults, our interferometry attempts to remove the 'wrinkles' due to near-surface effects from reflections on 3D seismic source gathers.

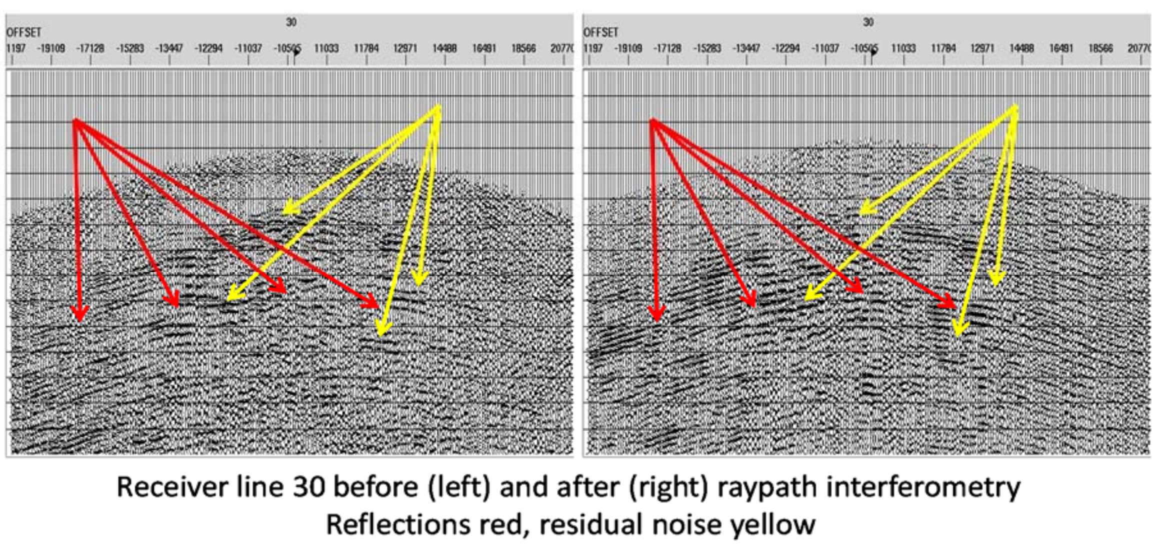

FIG. 1. A single receiver line from a large 3D source ensemble. Left: no surface corrections. Right: raypath interferometry applied to azimuth/offset-sorted ensembles using the Tau-P transform to move to and from the ray-parameter domain. Red arrows indicate reflection energy, which is much more coherent after interferometry; yellow arrows show coherent noise residuals, which are further reduced by the interferometry process.

Elastic microseismic full waveform inversion: synthetic and real data

Nadine Igonin† and Kris Innanen

ABSTRACT

In the microseismic and seismology field, determining the hypocenter of seismic events is necessary, and requires an accurate velocity model. In conventional FWI, one of the outputs is often a P- and/or S-wave velocity model obtained from (in most cases) sources on the surface. It is not difficult to imagine a framework where microseismic events could be used as additional subsurface sources that could increase the illumination in the reservoir. Furthermore, the velocity model obtained from such a scheme would be useful to re-locate said microseismic events more accurately. Therefore, this symbiotic relationship can be taken advantage of to formulate a FWI implementation where microseismic events are used to simultaneously update the velocity model, and the source position. This would involve two updates at each iteration - one for the velocity model and one for the source position. In this report, we explore in detail the source-term gradient in an elastic 2D formulation. We discuss the effect of the starting position, dominant frequency, moment tensor, and receiver geometry. Furthermore, we explore the impact of cross-talk due to having an incorrect starting velocity model. Finally, we end with preliminary results with a real dataset from the Horn River Basin, British Columbia.

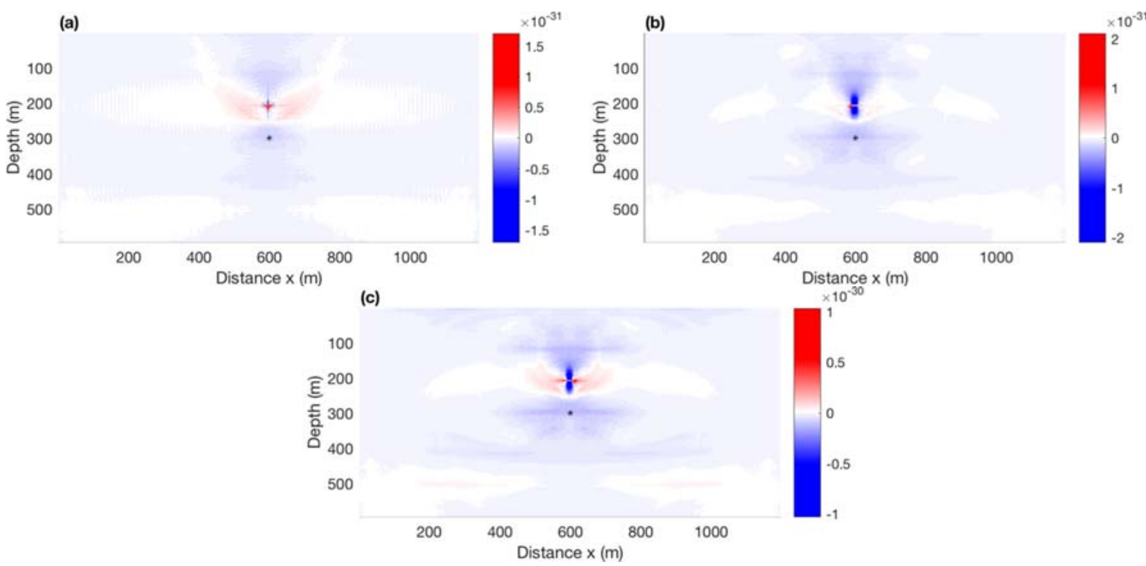

FIG. 1. Source-term gradient as a function of moment tensor with a(n) (a) explosive source, (b) double couple source, and (c) CLVD source after one iteration. Red stars indicate the maximum of the source-term gradient, and the black stars indicate the true source position. The starting source position is at the center of each dark blue region.

Design and deployment of a prototype multicomponent DAS sensor

Kris Innanen*, Don C. Lawton, Kevin W. Hall, Kevin L. Bertram, Henry Bland and Malcolm Bertram

ABSTRACT

In 2016-2017 CREWES published a range of analyses and applications of a geometrical model of fibre-optic (DAS) data for arbitrary fibre shapes. Amongst those applications was a multicomponent estimation scheme based on a careful accounting, and combined usage, of the varying fibre directions associated with a shaped cable layout. In 2018 a prototype shaped DAS fibre array ("the pretzel") was buried to put some of these ideas and their feasibility to the test. In October 2018 the pretzel was illuminated from several directions, and shot records were analyzed to assess whether commonly available directional sensitivity is sufficient to permit multiple components of strain to be estimated simultaneously. By picking a P-wave arrival and comparing it to an analytic model, we conclude with a cautious yes. Other important directionality conclusions are also derivable from this experimental setup; for instance, the polarity or first-motion ambiguity of DAS is clearly rendered in the data.

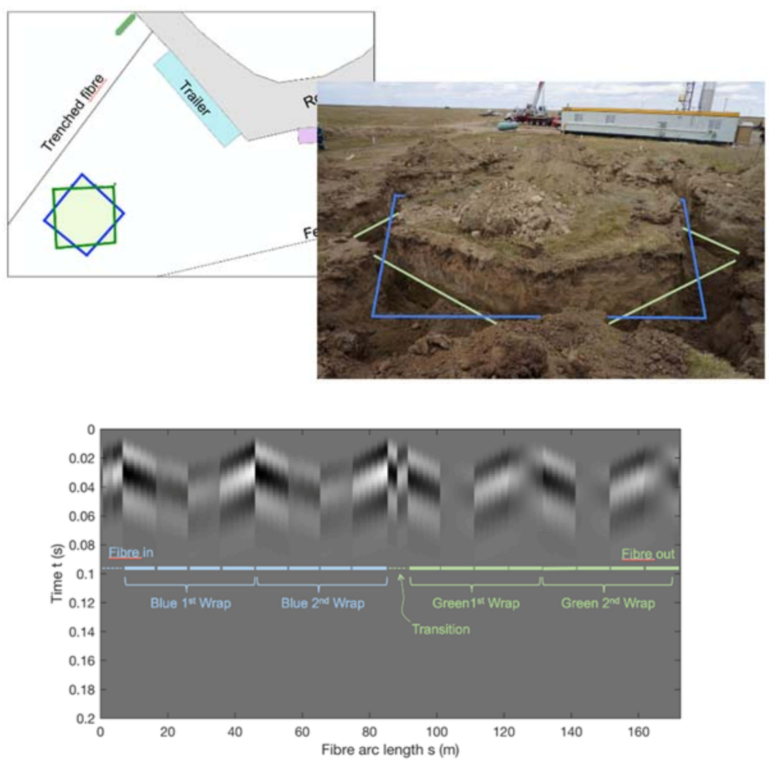

FIG. 1. A fibre array was trenched in at roughly 2m depth at the CaMI-FRS in September 2018 (top two panels). Intervals of the array were laid out such that elements with clear directional sensitivities were at least one gauge length long; thus the "sensor" is on the order of 10x10m laterally. This sensor was shot into from a variety of directions, and the field directionality was compared with modeled directionality (lower panel).

Elastic bracing and its effect on seismic waveforms in reservoir injection zones

Kris Innanen, Don C. Lawton, and Malcolm Bertram

ABSTRACT

Comparisons of seismic waveforms propagating through geological formations before and during injection of microbubble water and/or CO_2 are suggestive of dynamic effects that cannot easily be explained with normal linear elastic theory. A characteristic change in the coda, a strong loss of low frequency energy, and a moderate increase of high frequency energy have been noted. Rather than appealing to linear elastic wave theory coupled with an unrealistic level of new heterogeneity, we point out that homogeneous elastically-braced media produce all three of these features in a propagating waveform as first order effects. A modified Klein-Gordon equation is used to replicate behaviour in a published microbubble injection experiment, and similar features are sought in a raw VSP data set acquired before and during injection of CO_2 at the CaMI-FRS in November 2018. Early indications are that the two spectral changes explainable via Klein-Gordon waves can indeed be seen in the VSP data, but issues such as source coupling repeatability must yet be eliminated as factors.

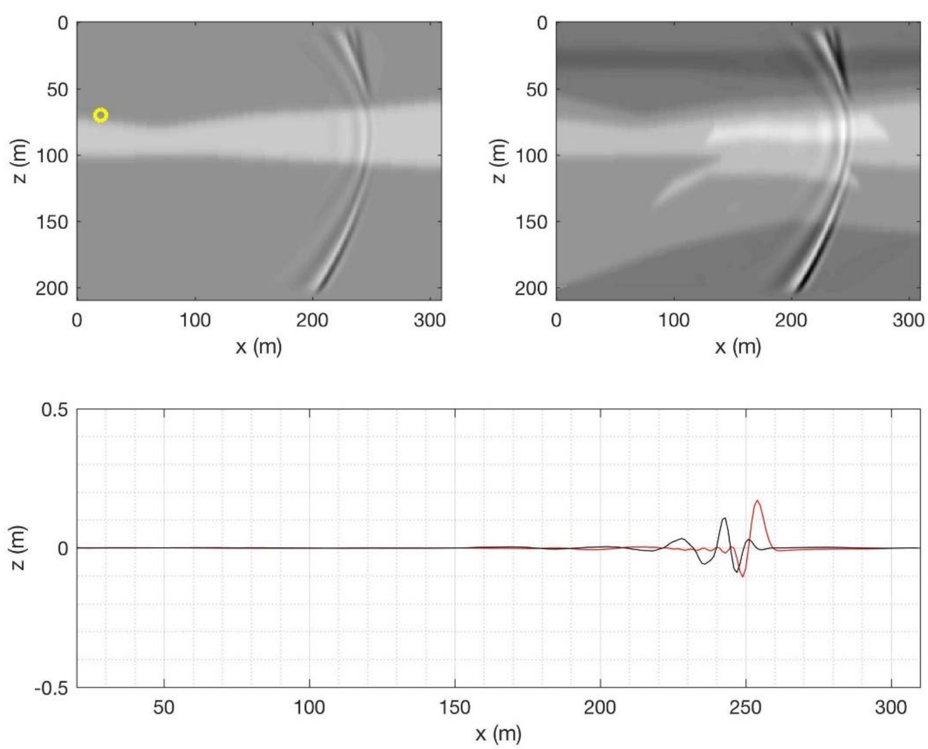

FIG. 1. Elastic wave propagation equations are modified to simulate elastic Klein-Gordon waves propagating through a scaled version of a published microbubble experiment. Top panels: snapshots of the KG fields during propagation; lower panel: comparison of wave fields propagating through standard elastic media (red) versus the KG alternative. The characteristic coda is visible.

Space-time boundary reflections in elastic media

Kris Innanen*

ABSTRACT

In 2017 potential monitoring applications of an unusual but perfectly real type of seismic reflection was discussed, namely that from time-boundaries (and mixed space-time boundaries). The idea is simply that reflections occur from jumps in medium properties, and this holds for jumps along the time coordinate axis just as surely as for jumps along one of the space coordinate axes. Time boundary reflections are intrinsically "normal incidence" scattering events. Analysis was carried out in order to plausibly discuss *oblique* time-boundary reflections; these were argued to be possible only if the boundary had both space and time components. In this short note we further this interpretation by demonstrating that if elastic waves (P- or S-) encounter pure time boundaries, no conversion occurs. However, if the boundary includes spatial variations as will as time variations, becoming, as it were, oblique time reflections, conversions do occur.

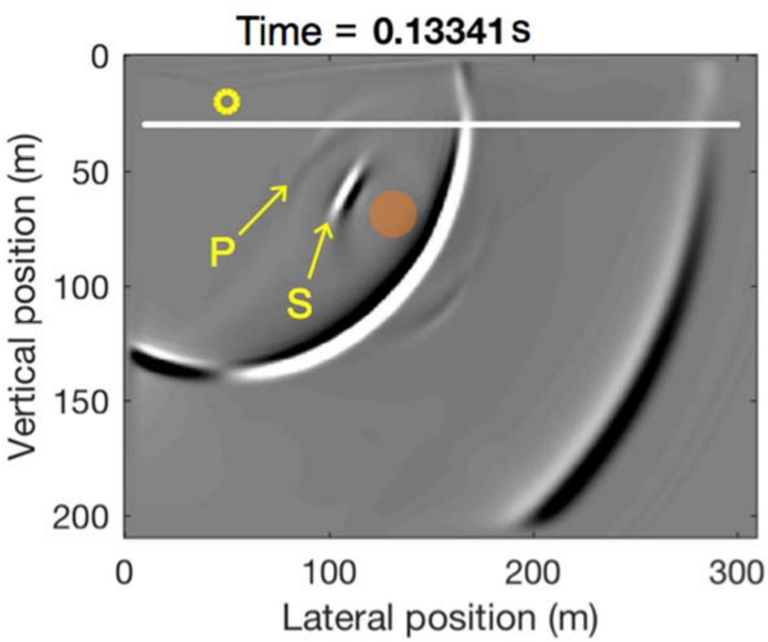

FIG. 1. An elastic wave interacts with a space-time boundary, namely a Gaussian shaped variation in medium properties appearing at t=0.13s, time to affect the slower S wave (orange circle). A short time later, two disturbances propagating back towards the source (yellow circle) are visible, one propagating at the P-wave velocity and the other at the S-wave velocity. Thus, an SS wave and a converted SP wave have both been created. In the comparable simulation wherein the entire volume undergoes the change (i.e., a pure time-boundary) only mode-conserved interactions take place.

Internal multiple prediction and subtraction: VSP, pre-and post-stack seismic data examples

Andrew Iverson*, Kris Innanen, Daniel Trad, and Marianne Rauch-Davies

ABSTRACT

A land dataset has been donated to CREWES due to a significant issue with internal multiples. This dataset includes well logs, a VSP and 3D seismic data. Synthetic modeling and tie to the 3D data demonstrate that internal multiple problems are present. A synthetic data test shows that inverse scattering series internal multiple attenuation can be used to remove some of the internal multiple energy. The learnings from this synthetic study are applied to both the VSP and 3D data. Extension to these data has proved to be challenging, though it is difficult to quantify results, and there are still learnings from the analysis. While there are minimal assumptions for the inverse scattering method, it is possible that that of low noise has been violated in this data set. Despite these difficulties there are locations throughout the 2D crossline test where there appear to be improvements in coherency, though this is largely a qualitative observation.

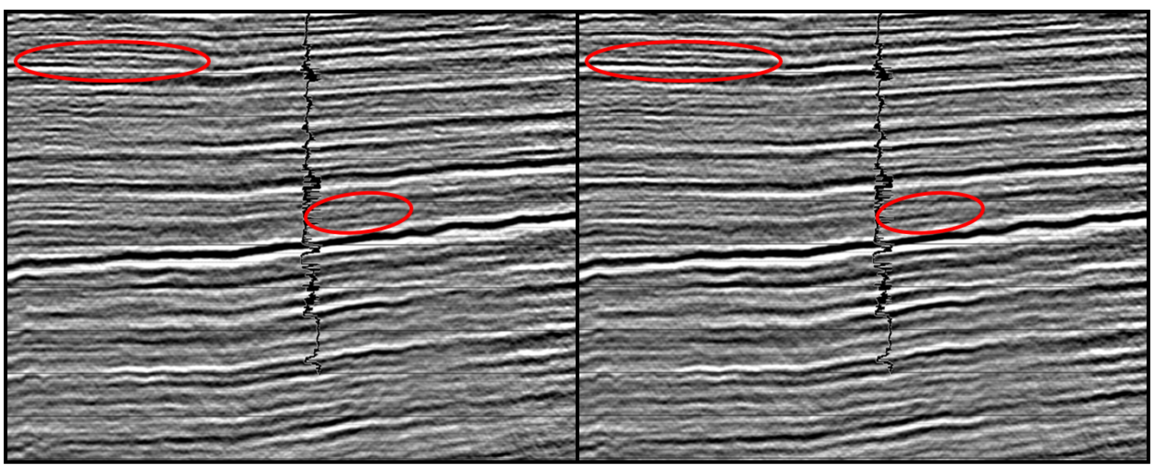

FIG. 1. (Left) Crossline through PSTM stack after internal multiple attenuation, with red ovals highlighting significant areas of change due to internal multiple attenuation. (Right) Crossline through PSTM stack.

Internal multiple prediction and subtraction: well log synthetic

Andrew Iverson, Kris Innanen, and Daniel Trad

ABSTRACT

Internal multiples can be a significant issue in the processing and interpretation of seismic data. The inverse scattering series internal multiple attenuation algorithm is used to predict and attenuate internal multiples. The algorithm has displayed success, especially in cases with separation between the primary and internal multiple events. A land dataset with a significant internal multiple problem has been donated to CREWES. The focus of this report is on synthetic tests created from the donated well logs prior to analysis of the donated seismic data. Several objectives are examined here, including confirmation of the multiple issue through modeling, and assessment of the applicability of the method to predict and attenuate internal multiples in this case. It is shown that a careful implementation of the method using 2D adaptive subtraction successfully attenuates internal multiples, even where there is significant overlap between primary and multiple energy.

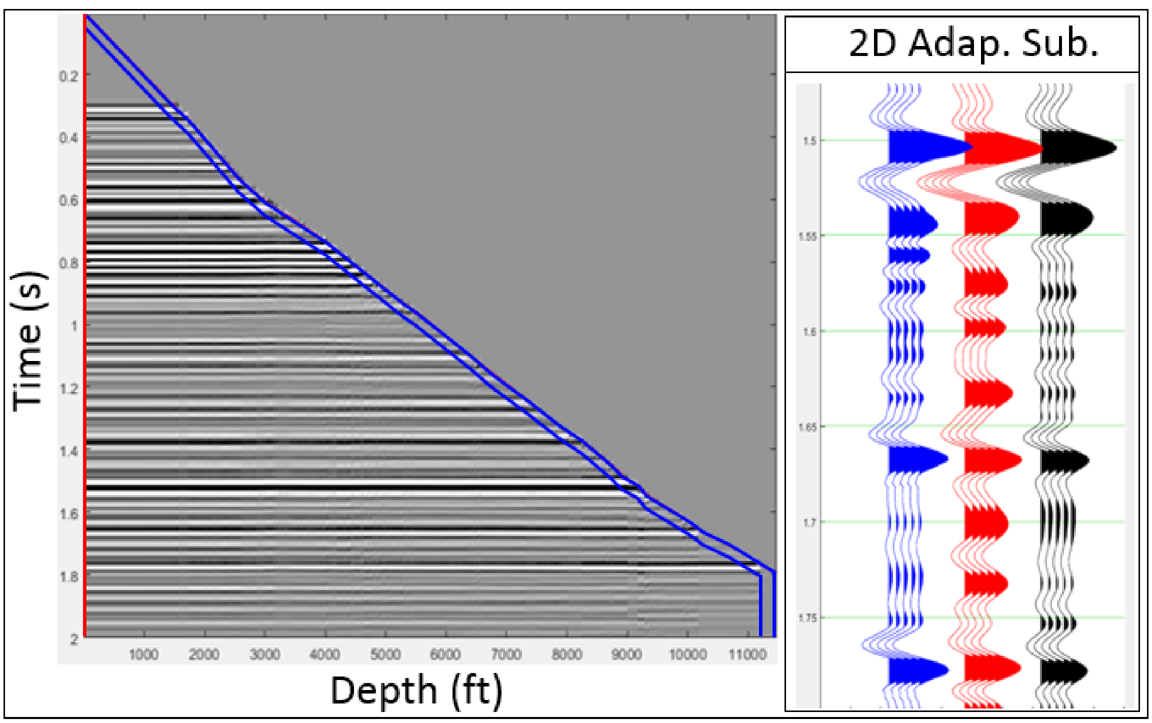

FIG. 1. (Left) Flattened synthetic VSP displaying outside corridor stack (primaries) in blue and zero depth trace (primaries and multiples) in red. (Right) outside corridor stack (primaries) in blue, zero depth trace (primaries and multiples) in red and zero depth trace after internal multiple attenuation in black.

Internal multiple prediction with higher order terms and a new subtraction domain

Andrew Iverson, Scott Keating, Kris Innanen, and Daniel Trad

ABSTRACT

Inverse scattering series internal multiple attenuation is a promising method for predicting and attenuating internal multiples. Though the method has displayed great potential, it is not a routine step in the seismic processing workflow. Some of the issues with the method include small errors with the predicted amplitudes, which are corrected with an adaptive subtraction. After subtraction, the question often arises whether primary energy is being damaged in the removal of internal multiples. A new domain to carry out the adaptive subtraction is introduced here, which may mitigate this risk. This domain is a more natural space to create the filter as systematic amplitude errors due to the prediction algorithm can be corrected in this space. To further assist the amplitude mismatches, additional terms from the scattering series are incorporated, and the importance of how these terms are implemented is discussed. Combining this higher dimensional adaptive subtraction space with the higher order terms significantly improves the accuracy of the prediction.

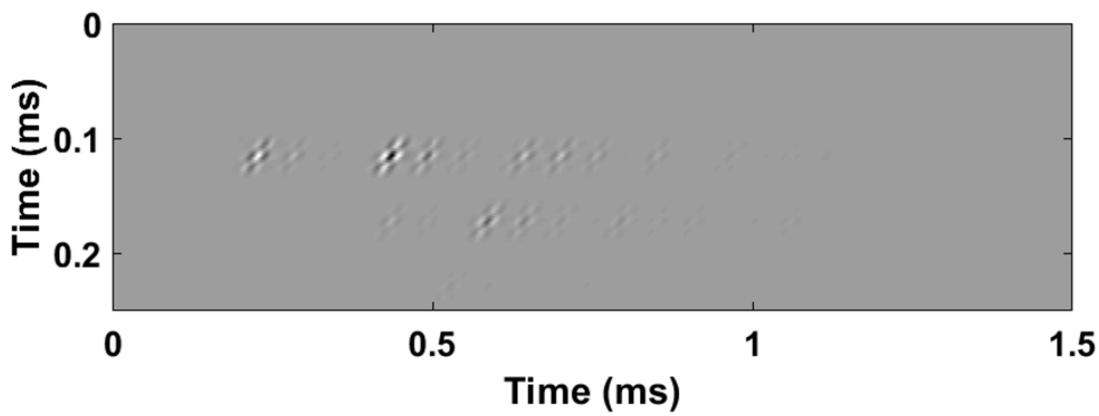

FIG. 1. 2D downward generator space displaying internal multiples as a function of downward generator time on the vertical axis

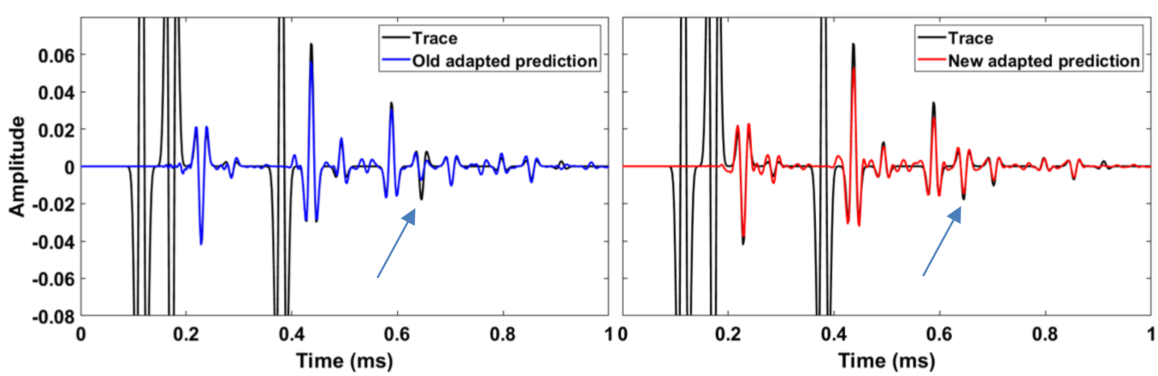

FIG. 2. (Left) Internal multiple prediction with 1D adaptive subtraction (Right) Internal multiple prediction with 2D adaptive subtraction.

Least-squares RTM of a seismic-while-drilling dataset

Nasser Kazemi*, Daniel Trad, Kris Innanen, and Roman Shor

ABSTRACT

Least-squares migration can, in theory, reduce the acquisition footprint and improve the illumination of the subsurface structures. It can also recover the amplitudes of the events to some extent. However, the migration operator is not complete. In other words, the operator does not span the full range of the model and the portion of the model that is in the null space of the operator will not be recovered even by posing imaging as an inverse problem. In geophysical terminology, in complex subsurface structures, rays or the wave energy will penetrate poorly in some regions, e.g., subsalt region, and that region will be a shadow zone to our acquisition system. The shadow zone is in the null space of the migration operator and the subsurface information in that region will not be recovered. Accordingly, in this research, we aim at using another set of dataset whose ray paths are different from the surface seismic. Seismic-while-drilling (SWD) datasets are complementary to surface data, and bring an opportunity to address seismic illumination issues by adding new measurements into the imaging problem. Provided that we understand the correlative and non-impulsive nature of the SWD source signature, the prestack least-squares depth migration of the SWD dataset (Figure 1) can be achieved. We study the feasibility of the least-squares reverse time migration of the SWD dataset and its potential in imaging the parts of the model which are in the shadow zone of the surface seismic acquisition.

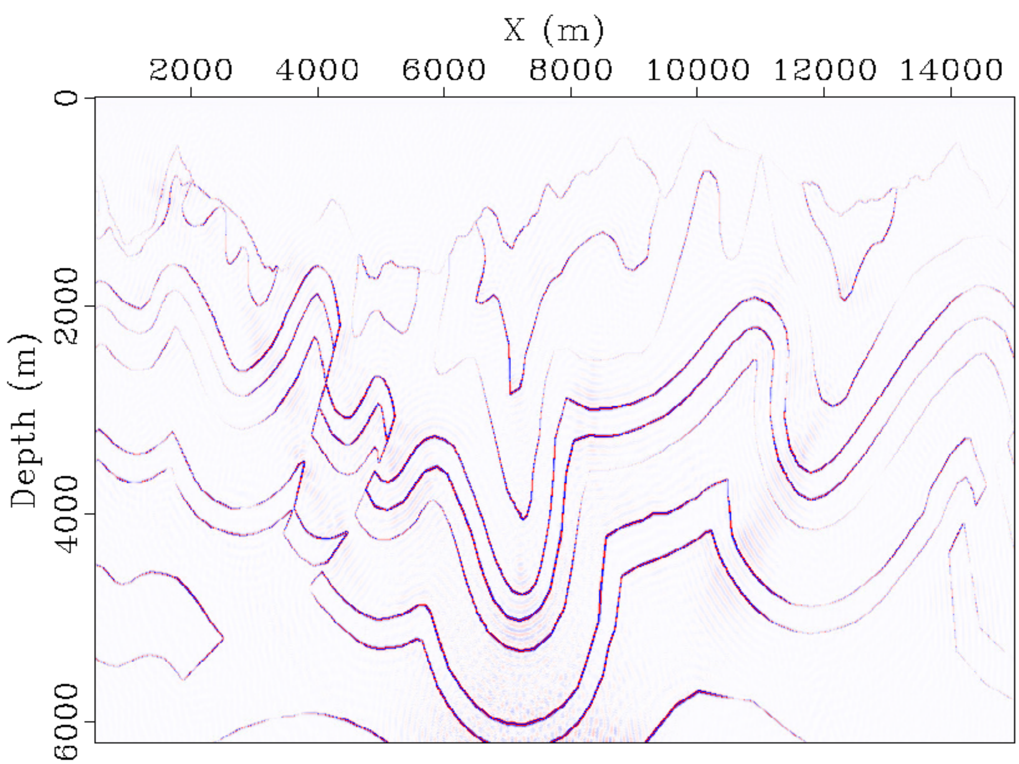

FIG. 1. Least-squares reverse time migration of the SWD dataset after 10 iterations.

A comparison of two reflection-based waveform inversion strategies

Scott Keating and Kris Innanen

ABSTRACT

Reflection-based waveform inversion is a set of strategies for updating the long-wavelength part of a velocity model through the use of reflection data in a full waveform inversion approach. Two analytical formulations of this type are proposed in this paper. A migration-based version uses a migration as the model of seismic reflectivity and directly calculates the effect of velocity model changes on this reflectivity. This approach is computationally intensive, and may estimate reflectivity poorly. The second approach considers only vertical shifts to a fixed reflectivity model. This reduces cost and allows for a better initial reflectivity model, but has the drawback of simplifying the effects of velocity model changes on the reflectivity. Neither approach uses demigration, instead using a long-wavelength model parameterization to ensure that reflectivities are not directly modified in the inversion.

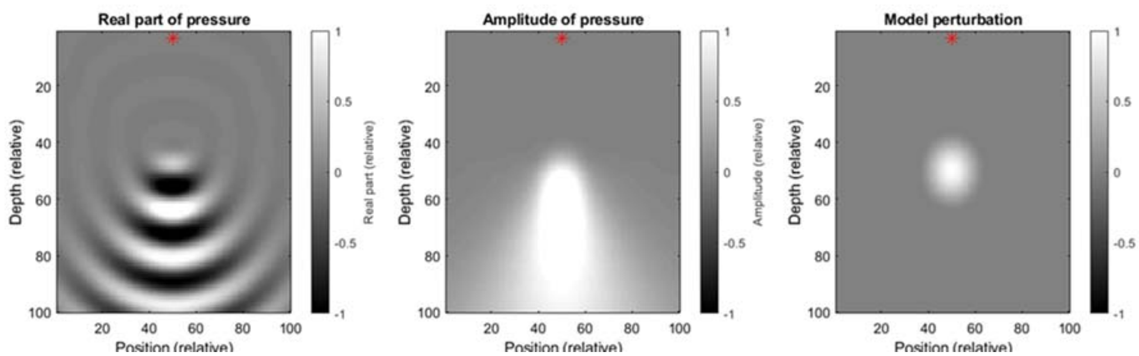

FIG. 1. Left: Real part of frequency domain radiation pattern. Center: Amplitude of frequency domain radiation pattern. Right: Variables considered in inversion. The red stars mark the source location. Changes in variables like this introduce limited reflections, allowing for the RWI strategy to be used without demigration. This should also allow for the natural treatment of diving waves simultaneously.

Connecting FWI and LSRTM through variable restriction

Scott Keating* and Kris Innanen

ABSTRACT

The imaging of seismic reflectors can be iteratively improved by using a least-squares migration (LSM) approach. Full waveform inversion (FWI) is usually posed as an inverse problem for the long to intermediate scale features of a seismic model, with little contribution from reflectors. Here, we show that full waveform inversion can be formulated to perform a similar role to LSM by choosing an appropriate choice of model parameterization. This approach specifically recovers the small wavelength features of the subsurface and does not require a complicated objective function or data filtering. Numerical tests show that this approach can be more effective than conventional FWI in recovering seismic reflector information.

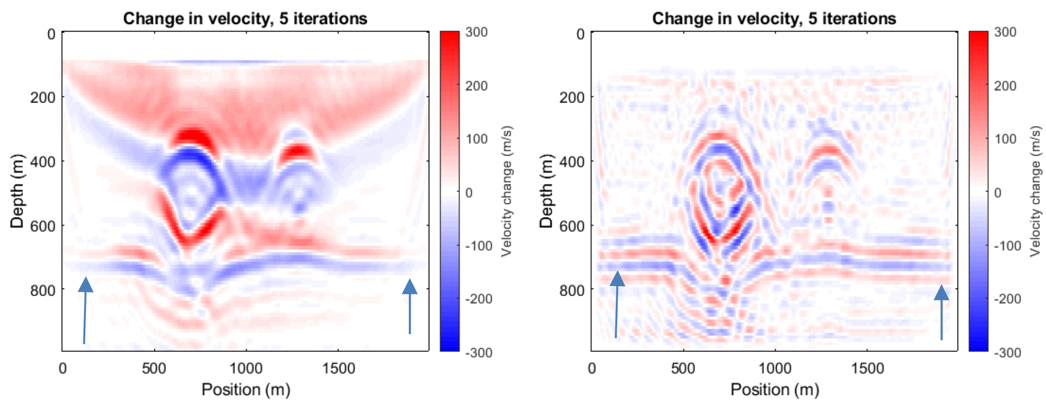

FIG. 1. Left: Conventional FWI result with poor starting velocity model after five iterations of BFGS optimization. Reflector recovery is limited at poorly illuminated edges. Significant long wavelength changes are introduced. Right: Variable restricted FWI with poor starting velocity model after five iterations of BFGS optimization. Reflector recovery at edges is substantially improved. Only short wavelength features are changed in the inversion.

Using multi-resolution truncated Newton optimization for cross-talk reduction in FWI

Scott Keating and Kris Innanen

ABSTRACT

Cross-talk, where data signatures of different physical properties are confused, is a major concern in multi-parameter FWI. This can be mitigated by using a good estimate of the Newton update in the inversion procedure, but such an approach is typically too computationally intensive to be pursued. In this report, the cost of approximating the Newton update is reduced by considering a multi-resolution approach, in which the grid defining the model is varied with frequency. This approach allows for a smaller computational burden at low frequencies, and effectively mitigates the cost of approximating the Newton update. This allows for cross-talk to be more effectively prevented.

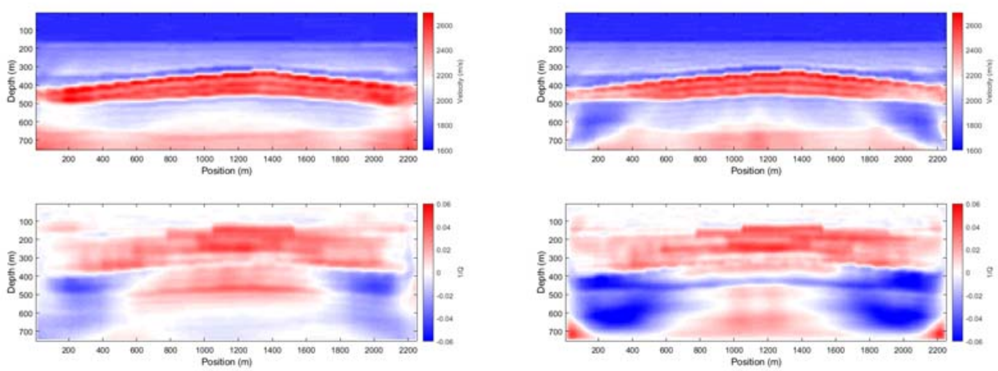

FIG. 1. Left: Multi-resolution truncated Newton FWI result for P-wave velocity (top) and Q_P (bottom). There is coherence of the lowest layer and limited negative Q artifacts. Right: Fixed resolution (conventional) truncated Newton FWI result for P-wave velocity (top) and Q_P (bottom). The lowest layer shows significant artifacts near the edges, and significant negative Q artifacts suggest severe cross-talk.

Viscoelastic FWI: solving for Q_P, Q_S, V_P, V_S, and density

Scott Keating*†, Junxiao Li, and Kris Innanen

ABSTRACT

Useful information about seismic amplitudes is often neglected or under utilized in full waveform inversion due to the common neglect of elastic of attenuative physics considered in the inversion. To make better use of measured data, we present a frequency domain, viscoelastic full waveform inversion. Inter-parameter cross-talk is demonstrated to be a major concern in this problem, not easily prevented through comprehensive acquisition geometry or relatively intensive numerical optimization. We propose a strategy for cross-talk mitigation based on prioritizing the transmissive effects of the Q variables.

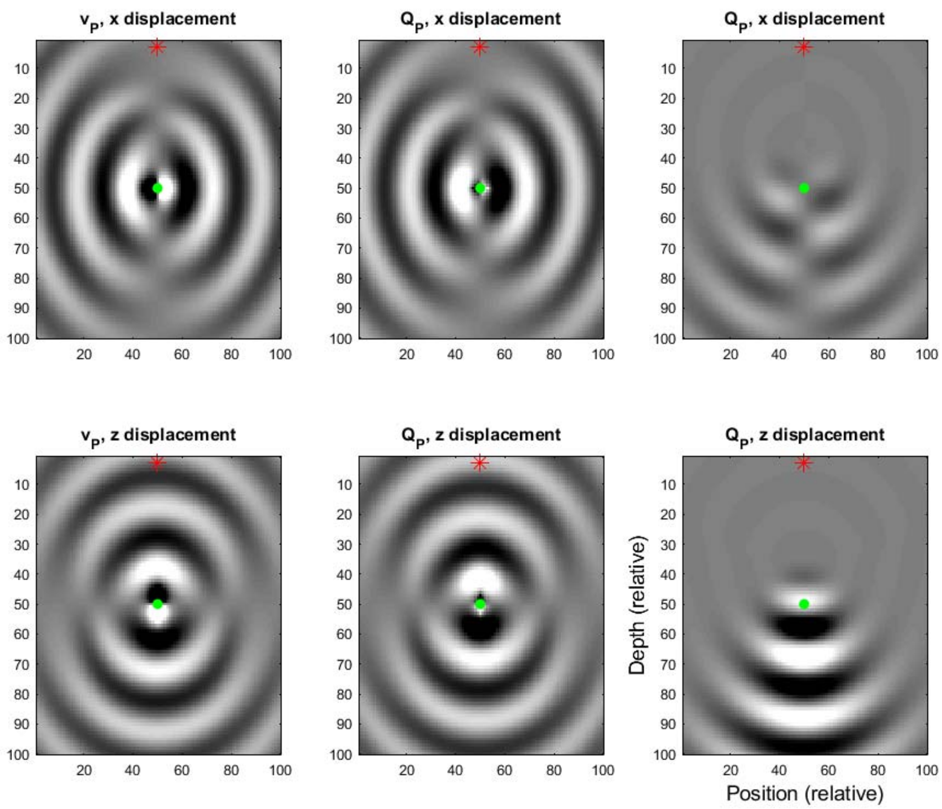

FIG. 1. Radiation patterns for different variables. The red star denotes the source position, the green dot is the location of the changed variable. Where these are highly similar for different variables, strong cross-talk is expected. Left: Radiation patterns for V_P parameter. Center: Radiation patterns for Q_P parameter with conventional FWI. Note the considerable similarity to the V_P pattern. Right: Radiation patterns for Q_P parameter with proposed strategy. Note that transmission effects dominate, little cross-talk is expected from reflections.

Jupyter notebooks and hubs for scientific computing

Michael P. Lamoureux† and Heather K. Hardeman-Vooys

ABSTRACT

The journal **Nature** recently published an article entitled *"Why Jupyter is data scientists' computational notebook of choice."* With three years of use under our belts, we discuss our experience with Jupyter notebooks, provide guidelines on how to make the transition to these tools for your own research, and present several useful resources to help you make this transition. As an illustrative example, we present a sample notebook recording our research efforts to achieve a 30x speedup in an implementation of standard finite difference code to numerically simulate acoustic waves in a variable velocity field, using WebGL on a GPU-powered video card.

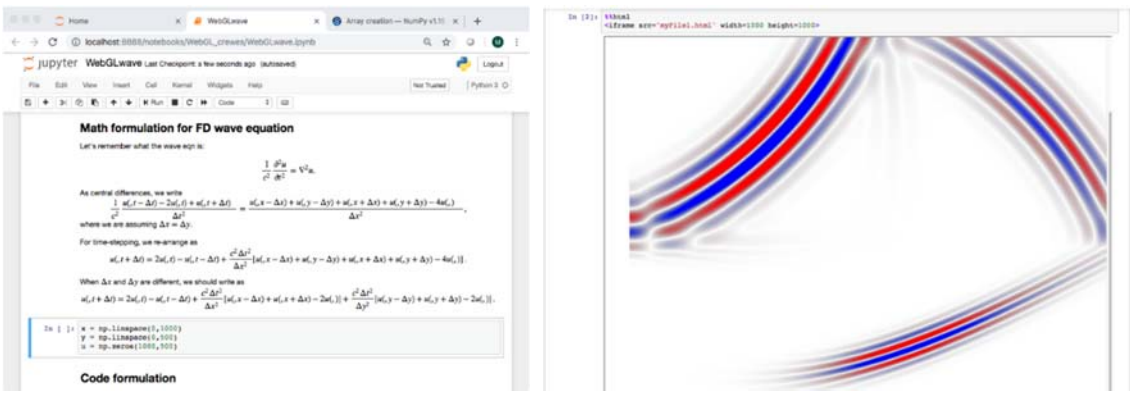

FIG. 1. (Left) Sample Jupyter notebook, combining text, formulas, data and code. (Right) GPU implementation of acoustic wave equation simulation, in a notebook.

Loop size	Matlab	C code	AMD-GPU	Nvidia-GPU	Speed-up
20,000	68 s	42.69 s	6.259 s	2.263 s	30x
40,000	137 s	85.37 s	11.919 s	4.285 s	31x
60,000	206 s	129.57 s	17.957 s	6.725 s	31x
80,000	275 s	180.82 s	23.844 s	8.873 s	31x
100,000	340 s	229.22 s	29.514 s	11.012 s	31x
Per iteration	3.41 ms	2.34 ms	.306 ms	.109 ms	31x

Table 1. Speed-up using GPU video card, in Jupyter notebook.

Velocity model building by slope tomography

Bernard Law*† and Daniel Trad

ABSTRACT

Slope tomography method uses slopes and traveltimes of locally coherent reflected events to estimate the macro velocity model from reflection data for depth imaging and full waveform inversion (FWI). Without the requirement of picking traveltimes on continuous reflection events, slope tomography is operationally more efficient than traditional reflection tomography. It is computationally more efficient than migration velocity (MVA), because it estimates the global velocity model simultaneously without layer stripping and expensive depth migration iterations. We review the slope tomography methods including CDR tomography, stereotomography and adjoint stereotomography.

Comparison of the slope tomography methods

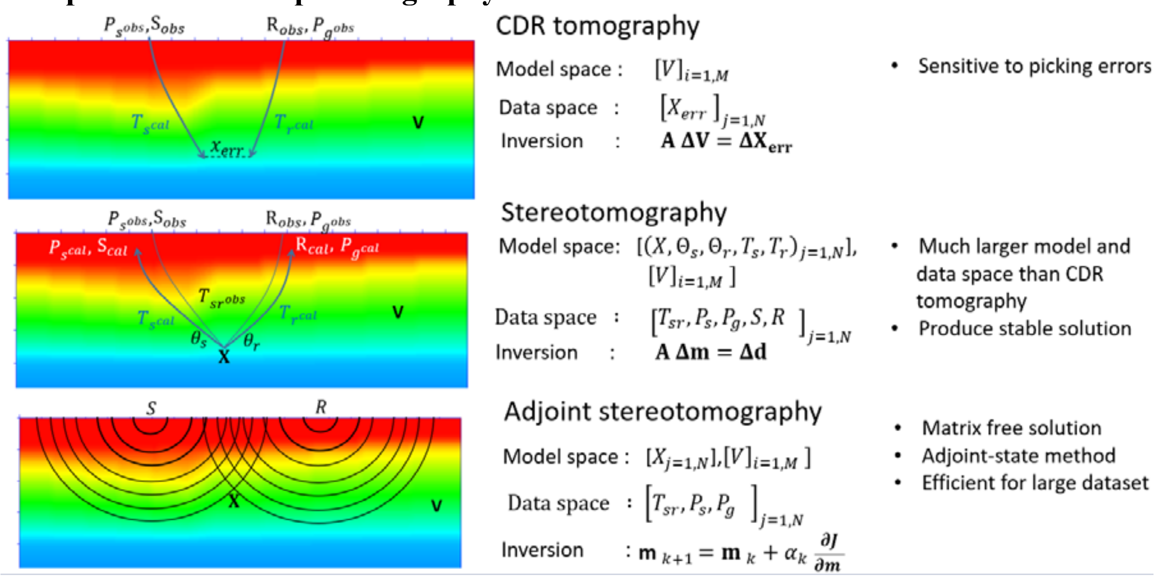

FIG. 1. Comparison of CDR tomography, stereotomography and adjoint stereotomography.

Numerical example

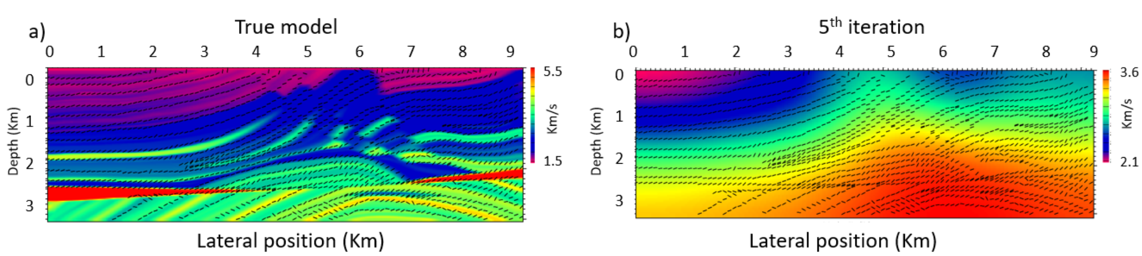

FIG. 2. (a) True velocity model and dip bars computed from CDR picks and CDR equations, (b) final velocity after 5 iterations using actual scatter positions.

Shear-wave studies of the near-surface at the CaMI Field Research Station in Newell County, Alberta

Don C. Lawton*, J. Helen Isaac†, and Malcolm Bertram

ABSTRACT

Two S-wave seismic surveys were acquired at the FRS in the summer of 2018 using Echo Seismic Ltd's shear-wave Envirovibe. For the first survey receivers were placed every 10 m in a fixed array and the source interval was 20 m. The second survey consisted of a 72 m streamer array towed behind the Envirovibe. The source interval was 2 m and the receiver interval was 1 m. The recorded S-wave data are of good quality with clear first breaks. Figure 1 shows the smoothed S-wave velocity model derived from refraction analysis. The near-surface S-wave low velocity layer is 28.5 to 34.5 m thick, with velocities ranging from 222 to 280 m/s. The S-wave bedrock velocity ranges between 1045 and 1110 m/s. The depths to bedrock compare well with the actual bedrock depth of 29.5 m at the injection well location. We applied some basic processing to both surveys, and stacked them. The streamer array line images the bedrock very well. This line was converted to depth (Figure 2) using the refraction velocities. The depth of imaged bedrock compares very well with the true bedrock depth of 29.5 m at the injection well.

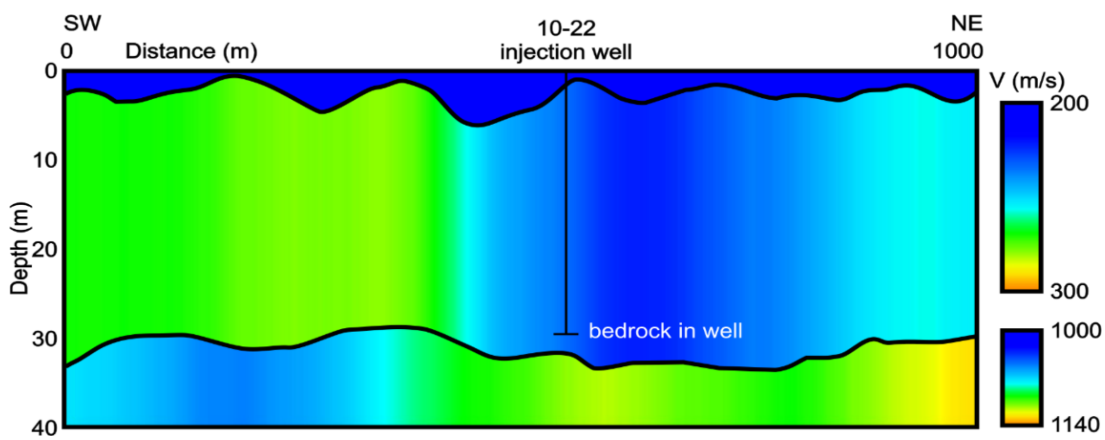

FIG. 1. Velocity/depth model derived from refraction analysis of the fixed array data.

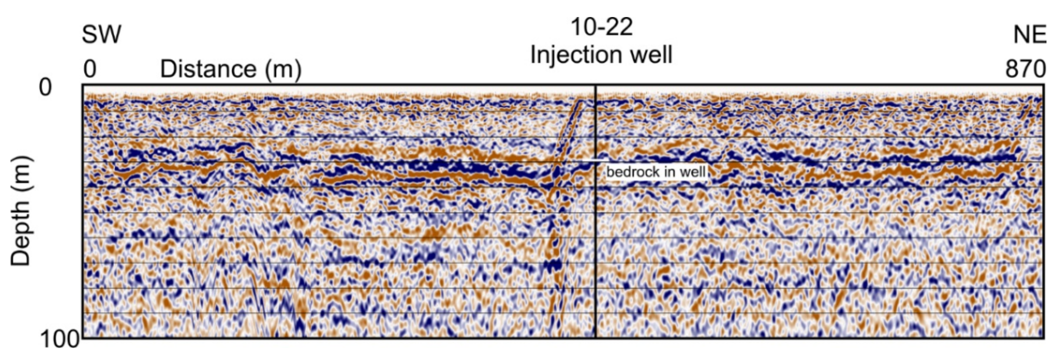

FIG. 2. The towed streamer S-wave section converted to depth. The imaged depth of bedrock compares very well with the actual depth of 29.5 m at the injection well location.

Phase unwrapping methods applied to data acquired using distributed acoustic sensing

Da Li, Heather K. Hardeman-Vooys, Raúl Cova, and Matt McDonald

ABSTRACT

PIMS Industrial Problem Solving Workshop in August 2018 offered a problem involving 2D phase unwrapping data acquired using distributed acoustic sensing (DAS). This report provides a summary of the work done during the week-long workshop. We begin with a description of the phase unwrapping problem. We consider the DAS dataset on which new methods were employed. We look at the results of the unwrap function found in MATLAB on the data and then provide a full description of two methods developed during the workshop. We then offer a comparison of the results from the two strategies.

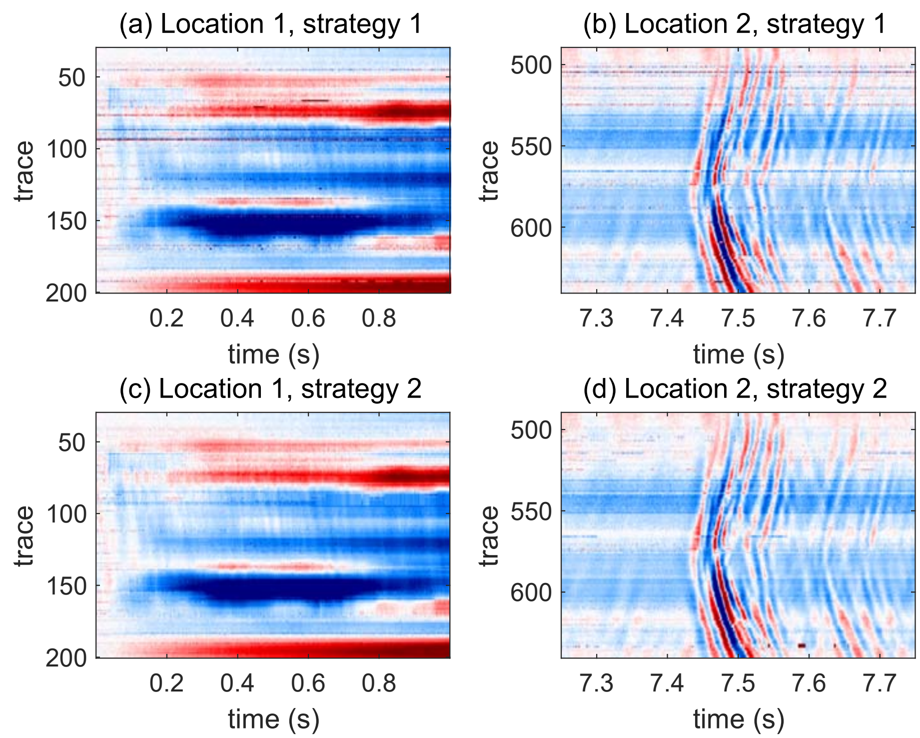

FIG. 1. The two strategies for unwrapping phase applied to two locations in the DAS dataset. (a) The results of strategy 1 applied to Location 1. (b) The results of strategy 1 applied to Location 2 in the data. (c) The results of strategy 2 applied to Location 1. (d) The results of strategy 2 applied to Location 2.

A 3D pseudo-spectral method for qP- and qSV- wave simulation in heterogeneous VTI media

Junxiao Li†, Huaizhen Chen, and Kris Innanen

ABSTRACT

During reverse time migration in anisotropic media, P- and SV-waves are coupled and the elastic wave equation should be used. However, the crosstalk caused by the interference between different wave modes is detected. Even if an acoustic anisotropic wave equation is used instead, an undesired SV-wave energy could be generated during modeling and reverse time migration. To avoid this unwanted energy, we proposed an approximation of decoupled P-and SV- wave equation system for vertical transversely isotropic (VTI) media. The qP- and qSV- phase velocities for the approximated equations are plotted and compared with the exact and other approximations, which proves its accuracy with different Thomsen parameter sets. The H-PML in second order wavenumber domain is also proposed to eliminate the artificial boundary reflections, comparisons of different absorbing boundary layers are also illustrated to validate the wave number domain H-PML.

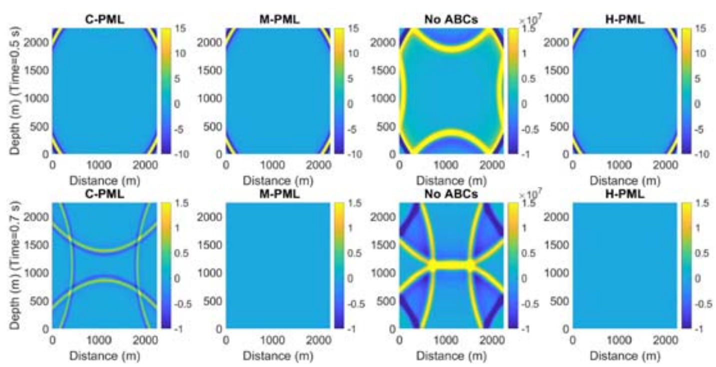

FIG. 1: Snapshots obtained by different boundary conditions.

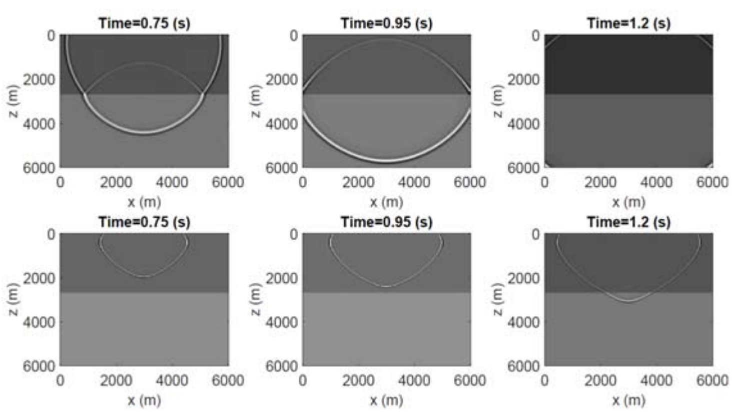

FIG. 2. The normalized decoupled qP-(Upper row) and qSV-(lower row) wavefield snapshots for a two-layer.

Parameterization of frequency domain FWI

Junxiao Li, Kris Innanen, and Wenyong Pan

ABSTRACT

Full-waveform inversion (FWI) aims to update the long and short wavelengths of the perturbations, in which parameterization plays an important role in multiparameter updates. For the anisotropic inversion of a transversely isotropic medium with a vertical symmetry direction (VTI), the parameterization can be chosen as five elastic constants (c_{11}, c_{13}, c_{33}, c_{44} and density) or in other forms of parameterizations. In this paper, a choosing of parameterizations is briefly discussed. The gradients of parameters (vertical P-wave velocity, horizontal P-wave velocity, vertical S-wave velocity and delta) are calculated. The comparison with the inversion of elastic constants demonstrates the inversion of Thomson parameters reduces interparameter crosstalks. To enhance the inversion results, the frequency-selection strategy is also applied, moving from lower to higher frequencies. The parameters sensitive to the low frequency are updated first, which are then used in other parameters.

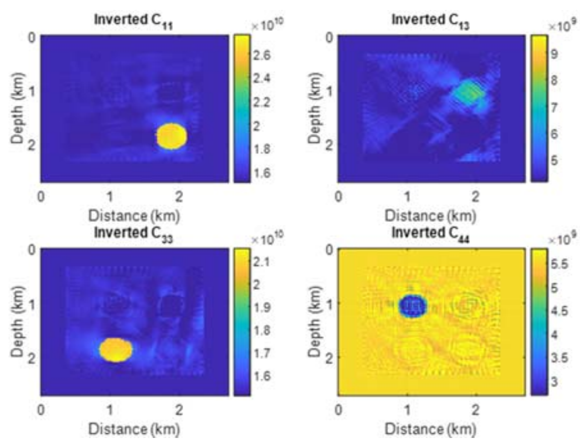

Fig. 1: Inversion results for elastic constants.

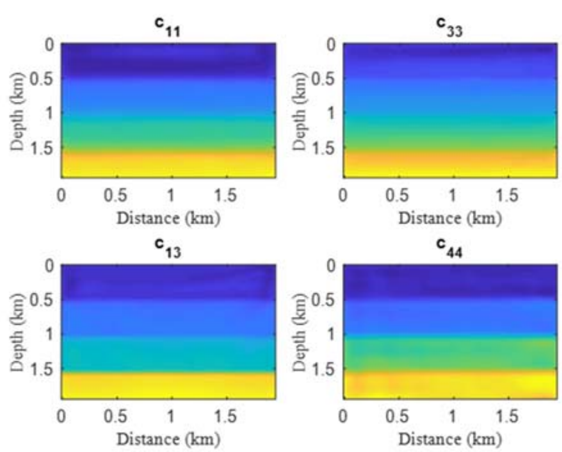

Fig. 2. Inversion results using frequency-selection strategy.

Symbiosis between geophysics and medicine

Laurence R. Lines*†

ABSTRACT

The fields of geophysics and medicine are widely regarded as important, and these fields have many similarities and differences. In evaluating their characteristics, there is the compelling question of whether there are potential symbiotic ideas in which either field may benefit from the other. The areas of imaging and vibrational pulsation are examined as areas of overlap and symbiosis. The noun "symbiosis" can be defined as "an interaction between two different organisms living in close physical association, typically to the advantage of both", according to Wikipedia. An area of common interest includes the imaging of a body's interior by the analysis of physical waves that have passed through the body. Geophysical and medical imaging have their similarities and differences other than the fact that in the case of geophysical imaging we hope to discover anomalies whereas in medical imaging, we generally hope to not find anomalies in the human body. In this article, I compare and contrast these imaging methods.

This talk explores tomography and reflection imaging (in both acoustical and electromagnetic imaging) in geophysics and medicine. Different algorithms must often be used in geophysics compared to medical imaging due to an incomplete aperture and ray bending (creating a nonlinear inverse problem). In both fields, reliable images can be obtained. Figure 1 (left) shows an ultrasound image of a human fetus basically using reflection seismology on the human body. Figure 1 (right) shows the superposition of a velocity tomogram on a depth migration for a Gulf of Mexico salt intrusion. The images use similar acoustical imaging methods on reflection data to obtain useful information of a body's interior as derived from wave information. It is proposed that similar signal processing methods can be used to improve both medical and seismic images.

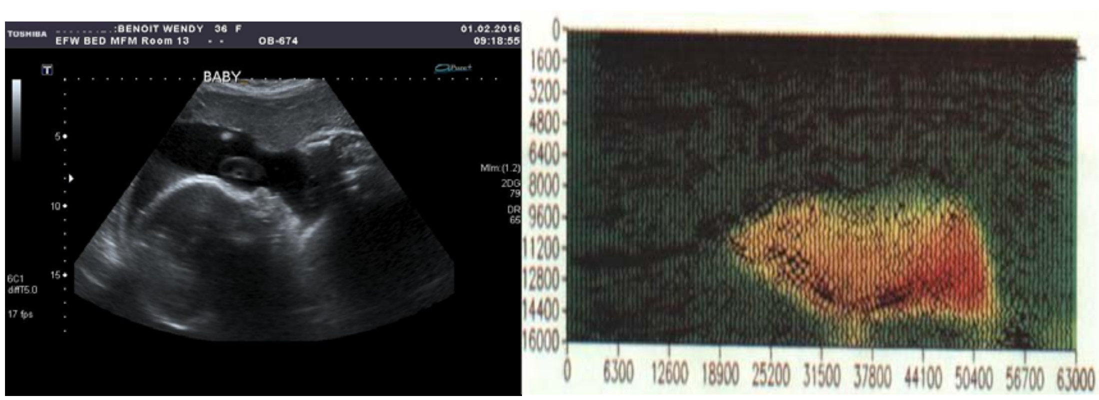

FIG. 1. (left) An ultrasound image showing the head of my granddaughter Alice Benoit about 8 weeks prior to birth. This image was provided courtesy of her mother, Wendy Benoit. (right) A depth image of a Gulf of Mexico salt intrusion from Lines (1991). Both results were obtained using reflection imaging methods.

Ambient noise correlation study at the CaMI Field Research Station, Newell County, Alberta, Canada

Marie Macquet*† and Don C. Lawton

ABSTRACT

At the CaMI Field Research Station we recorded several weeks of continuous surface and borehole seismic data to study the feasibility of using ambient noise correlation (also called interferometry) to monitor CO_2 injection. We focus here on the October 2017 dataset (prior to injection), composed of 14 days of continuously recorded data at the 98 stations of a 3C-3D permanent array (receiver grid of 10 m x 10 m). We use a standard processing (mean and trend removal, 1bit, spectral whitening) and compute the 14 daily ZZ-correlations for the 4753 pairs of stations to reconstruct the Green's function between them. Daily correlations show stable waveform for the baseline dataset with a good correlation coefficient between the reference and the daily correlations (Figure 1). Variations in the elastic parameters of the subsurface due to CO_2 injection will directly affect the reconstructed Green's function, and passive recording should allow us to detect the induced change of the medium. Interferometry can also be used as a tomographic tool through the analysis of the dispersion curve of the reconstructed Green's functions. Figure 2 shows the dispersion curve obtained for a couple of stations located 80 m apart. A detailed analysis will be undertaken to determine why some periods show outlier values, but the group velocities obtained are similar to those found in literature.

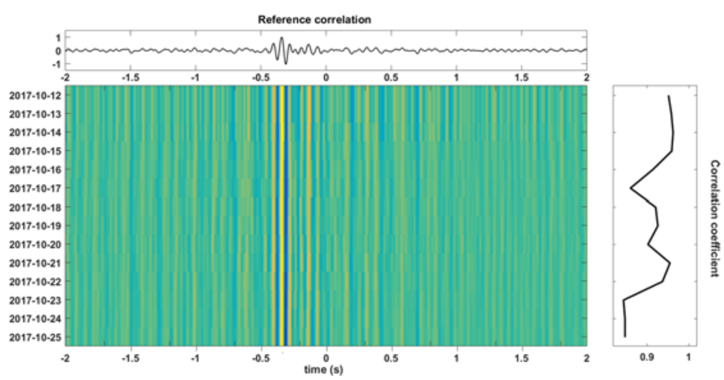

FIG. 1: Stability of the correlation between the station 1009 and 9001 (80m apart). Top: Reference correlation (14 days stacked). Middle panel: Interferogram of the daily correlations. Right: Correlation coefficient between the reference correlation and the daily ones.

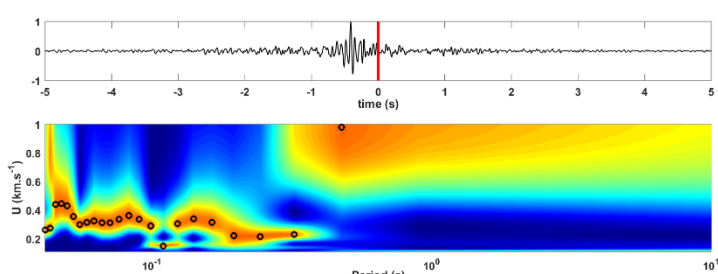

FIG. 2. Example of a computed group velocity dispersion curve for the 1001-9009 station pair (80m apart).

Pure P- and S-wave elastic reverse time migration with adjoint state method imaging condition

Jorge E. Monsegny*† and Daniel Trad

ABSTRACT

We implemented an elastic reverse time migration based on a coupled system of pure P- and S-wave particle velocities. The system utilizes finite difference wavefields for P- and S-wave particle velocity in vertical and horizontal directions (v_{xp} , v_{zp} , v_{xs} and v_{zs}), and for 2-D displacement divergence and curl (A and B). In contrast with the usual elastic imaging conditions that cross-correlate vertical displacements to obtain the P-wave image and vertical and horizontal displacements to obtain the converted wave image, we devised P- and S-wave imaging conditions using the adjoint state method. The resulting imaging conditions cross-correlate spatial derivatives of A and B wavefields with P- and S-wave displacements. The proposed migration shows a better reflector definition and more balanced amplitudes than the usual vertical and horizontal particle displacement cross-correlations.

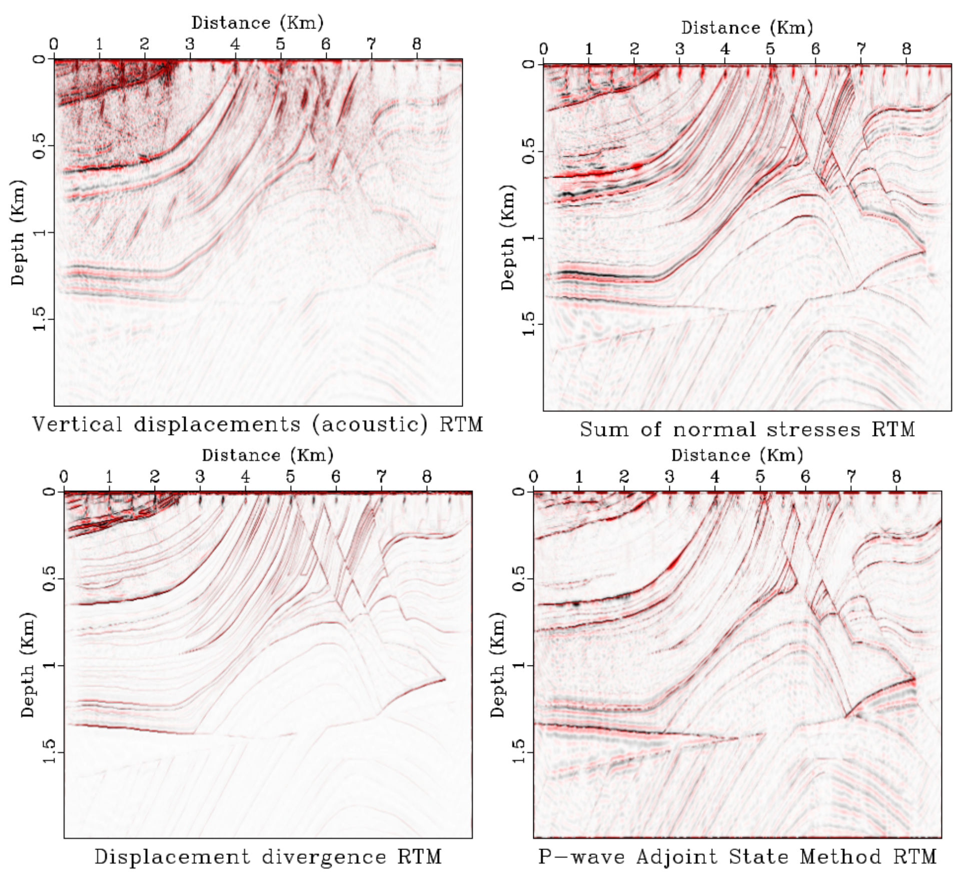

FIG. 1. In the top row are the vertical displacement cross-correlation RTM, and the elastic sum of normal stresses RTM. The bottom row shows the displacement divergence cross correlation RTM and the P-wave adjoint state method RTM. All migrations are normalized by the wavefield energy and have a Laplacian filter applied.

Azimuthally-dependent scattering potentials and full waveform inversion sensitivities in low-loss viscoelastic orthorhombic media

Shahpoor Moradi† and Kris Innanen

ABSTRACT

Determination by seismic full waveform inversion (FWI) of the anisotropic and attenuative properties of a geological volume, is a challenging task. One of the challenges is that seismic amplitudes are co-determined by the simultaneous variations of several properties, and the separation of these mixing effects is a complex and generally ill-posed problem. To optimally formulate multi-parameter updates in FWI, detailed parameter resolution analysis is required. Quantitative predictions regarding the resolution of any set of parameters can be made based on the scattering radiation patterns generated by local changes in medium parameters. Radiation patterns are computed via the Born approximate model of volume scattering. Scattering amplitudes as a function of opening angle provide information regarding the variations two independent parameters will cause in the data; if they are similar in character over some range of opening angles, one concludes that the two parameters will be difficult to distinguish with data spanning that angle range. For example, Figure 1 shows the radiation patterns generated by anisotropic parameters inserted in an isotropic background as a function of the opening angle for different azimuth angle.

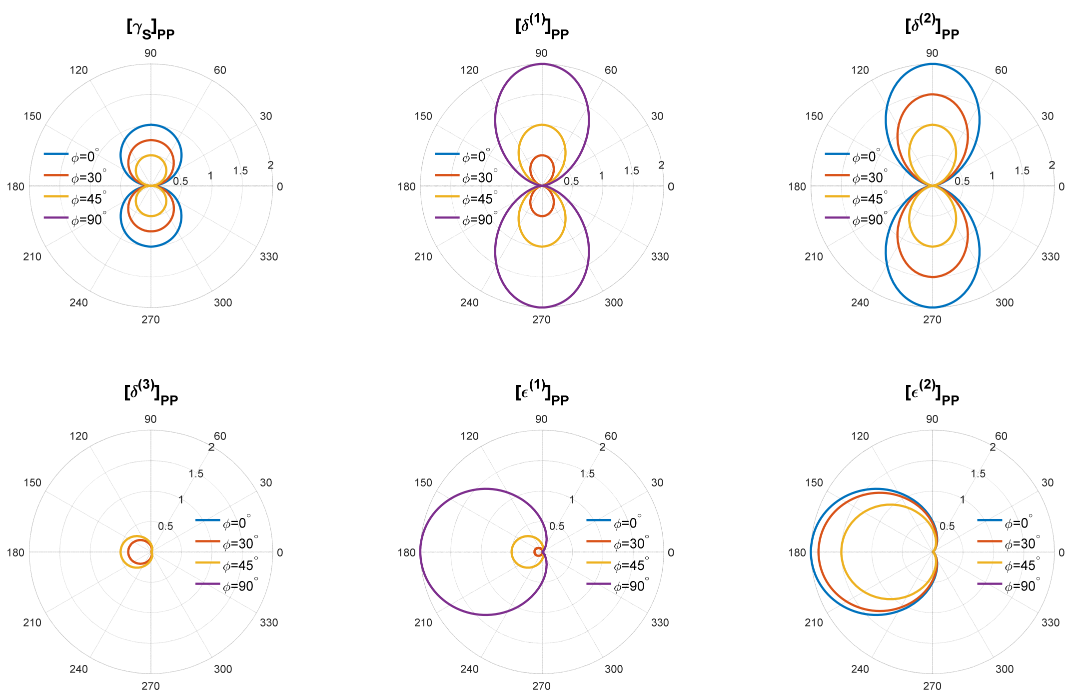

FIG. 1. P-to-P radiation patterns induced by anisotropic parameters versus opening angle (sum of incident and scattered angles).

Implementation of quantum algorithms in seismic modeling and imaging

Shahpoor Moradi*, Daniel Trad, and Kris Innanen

ABSTRACT

Recent advances in quantum computing hardware offer opportunities to explore solutions to real-world problems using quantum algorithms. Whether providing solutions more quickly or more accurately, quantum algorithms offer new methods for processing information that take advantage of quantum mechanical phenomena, including tunneling, entanglement, and superposition. Our goal is to design quantum algorithms to solve the expensive computational problems in exploration seismology, such as 3D wave modeling, seismic depth imaging, and elastic Full Waveform Inversion. Utilizing quantum information may substantially reduce the memory required to store the data or speed up the computational time of the algorithms by quantum superposition.

Figure 1 illustrates the simple example of a scatter point imaging in a homogeneous background (left). The image is a $N \times N$ matrix with nonzero components at the location of scatter point (middle). In quantum setting this matrix can be transformed into a N^2 dimensional vector with a probability distribution (right). Our model is 350×350, so the quantum state corresponds to the image has components in order of 10^5. To store this image on a quantum computer we need roughly 17 qubits. Due to the nature of quantum mechanics, at the end of computation, the image would be a quantum state of $\log_2 N$ quantum bits (atoms), all correlated to each other. This quantum state encodes the components of the $N \times N$ matrix representing the image. The location of the scatter point is characterized by the components with greater probabilities.

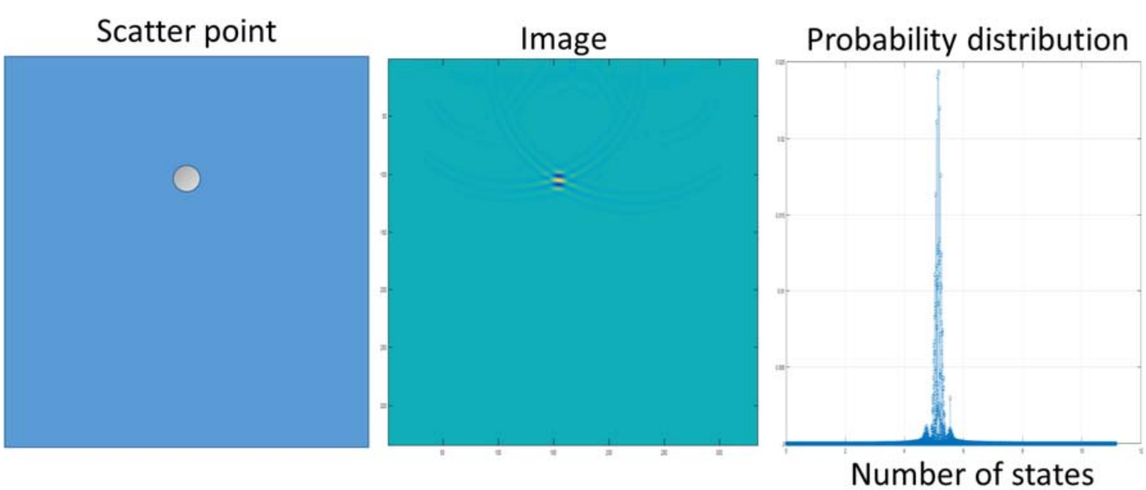

FIG. 1. Probabilistic interpretation of seismic imaging in quantum domain.

Inversion with the Born approximation in a deep learning framework

Zhan Niu†, Jian Sun, and Daniel Trad

ABSTRACT

Least square reverse time migration (LSRTM) has been an important technique that is favourable in the industry for several years. LSRTM is considered to have less computational cost than the Full-waveform Inversion (FWI) while maintaining good accuracy. Machine learning, on the other hand, has gained its attention in the geophysical area and has become one of the most booming subjects in computer science. Various tools and methodology have been developed. In this report, we first introduce an implementation of the Born modelling using the recurrent neural network (RNN) and second, we perform an inversion of the model by training the RNN with generated data. The inversion process can be proven to be same as LSRTM. The performance of different optimizers is compared and discussed. We conclude that the Adam optimizer is the most stable and time efficient for this method.

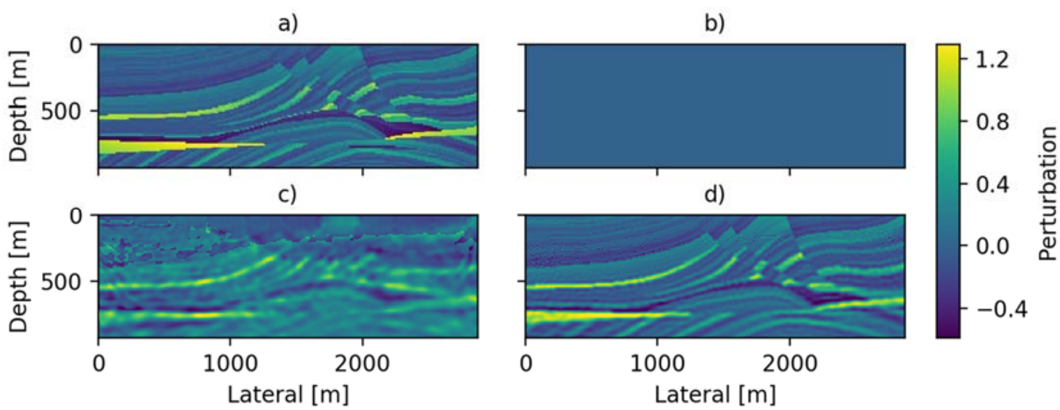

FIG. 1. The inversion results of Marmousi model by RNN. a) The true model; b) The initial model at all zeros; c) The model at the 10th iteration with Adam optimizer using learning rate 0.3; d) The model at the 50th iteration.

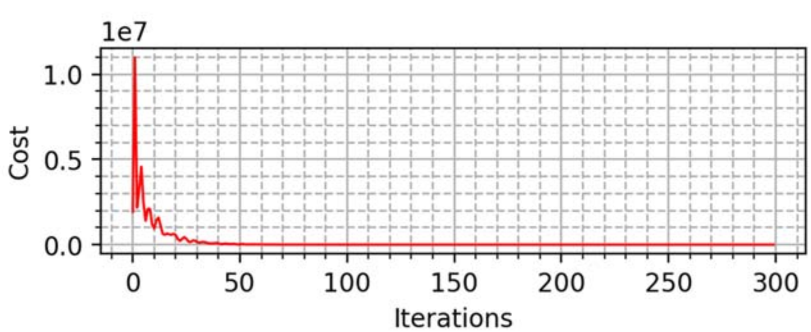

FIG. 2. The cost evolution through iterations on Marmousi model.

Elastic full-waveform inversion in attenuative and anisotropic media applied to walk-away vertical seismic profile data

Wenyong Pan and Kris Innanen

ABSTRACT

Viscoelastic full-waveform inversion (FWI) is applied to walk-away vertical seismic profile (W-VSP) data acquired at a producing heavy-oil field in Western Canada, for the determination of subsurface velocity models (P-wave velocity α and S-wave velocity β) and attenuation models (P-wave quality factor Q_α and S-wave quality factor Q_β). To mitigate strong velocity-attenuation tradeoffs, a two-stage approach is adopted. In stage-I, α and β models are first inverted using a standard waveform-difference (WD) misfit function. Following this, in stage-II, different amplitude-based misfit functions are used to estimate the Q_α and Q_β models. Compared to the traditional WD misfit function, the amplitude-based misfit functions show stronger sensitivity to attenuation anomalies and appear to be able to invert Q_α and Q_β models more reliably in the presence of velocity errors. Overall, the root-mean-square amplitude-ratio and spectral amplitude-ratio misfit functions outperform other misfit function choices. In the final outputs of our inversion experiments, significant drops in both α to β ratio (~ 1.6) and Poisson's ratio (~ 0.23) are apparent within the Clearwater formation (depth ~ 0.45-0.5 km) of Mannville Group in Western Canada Sedimentary Basin. Strong Q_α (~ 20) and Q_β (~ 15) anomalies are also evident in this zone. These observations provide informative inferences to identify the target attenuative reservoir saturated with heavy-oil resources. In the final section of this report, anisotropic-elastic FWI in vertical transverse isotropic (VTI) media with different model parameterizations are applied to this W-VSP data.

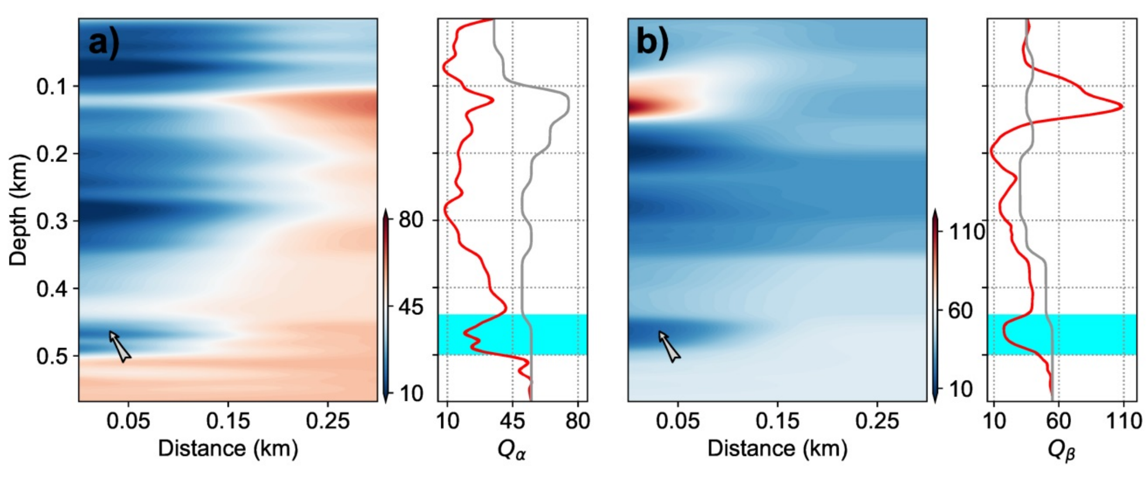

FIG. 1. (a) and (b) are the inverted Q_α and Q_β using the RMS-AR misfit function.

FWI with PSPI gradient: data validation vs well validation vs well-and-data validation

Sergio Romahn and Kris Innanen

ABSTRACT

Conventional acoustic full waveform inversion (FWI) involves the cross-correlation of the back-propagated data residuals with the forward-propagated source to produce the gradient. This process can be seen as the reverse time migration (RTM) of the data residuals. The gradient then is scaled to create a velocity perturbation. This step is achieved by applying a line search of the step length in a typical gradient descent scheme. We used PSPI, a wave equation migration method, to obtain the gradient, and we compared three different ways to produce the velocity perturbation. Firstly, we used a line-search method to scale the gradient, a process called data validation. Secondly, we applied well calibration, a technique that is called well validation. Finally, we used a combination of well and data validation. We applied these techniques to two different models, one with moderate lateral velocity changes, and the other one to the more complex Marmousi model. For a simple geological setting the three techniques provided similar results. Well and data validation produced the best result in the presence of more complex geological settings.

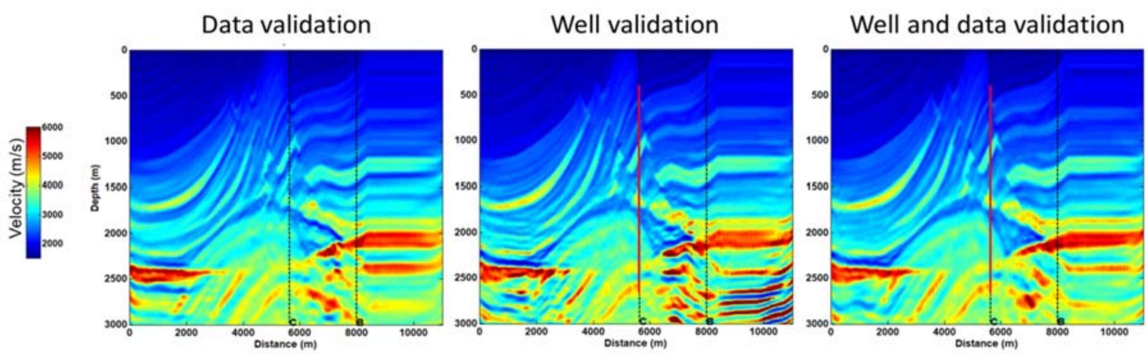

FIG. 1. Performance of data validation, well validation and well-and-data validation applied on Marmousi model.

Log-validated FWI with wavelet phase and amplitude updating applied to Hussar data

Sergio Romahn*† and Kris Innanen

ABSTRACT

The estimation of the wavelet that is used for forward modelling of synthetic shots is one of the main challenges that we must face when applying FWI in real data. We show the negative effects of an incorrect wavelet and propose a methodology to mitigate this problem in this report. We apply PSPI migration with well calibration instead of RTM and line search to produce the velocity perturbation. The use of PSPI reduces the computational time, and we take advantage of this fact to implement our methodology. The process starts with an estimated wavelet with similar frequency content as the seismic data. This wavelet does not have the optimal amplitude and phase for reproducing the observed shots. In order to address this problem, we migrate and stack the observed and modelled shots separately. Then we convert both data sets from depth to time by using the current velocity model. The comparison of these data sets in time domain provides the elements for the estimation of an amplitude and phase that make the modelled data more similar to the observed data. Next, we take the difference between the observed and corrected synthetic data to create the gradient. Finally, we calibrate the gradient with well information to produce the velocity perturbation. The amplitude and phase corrections estimated in this way are used to update the wavelet that will be used in the next iteration. We applied this methodology on synthetic and Hussar data, obtaining encouraging results.

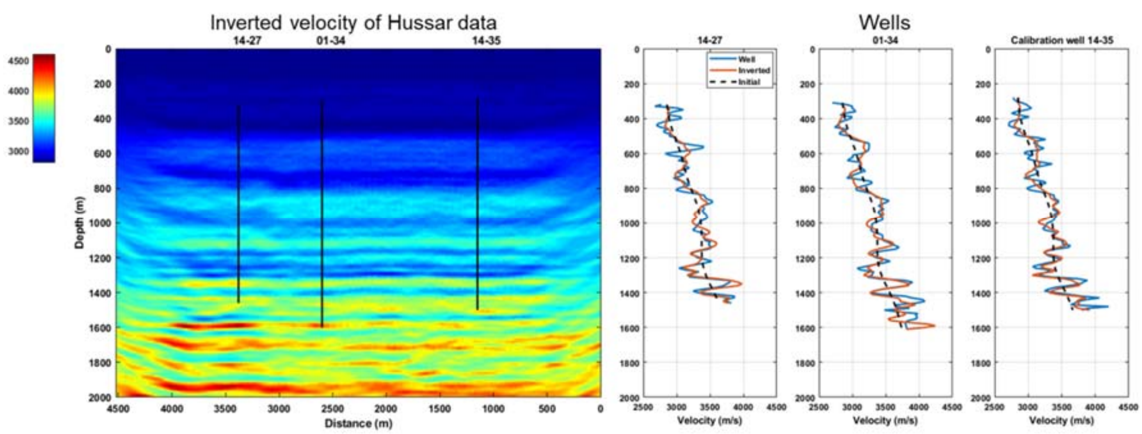

FIG. 1. FWI with amplitude and phase updating applied to Hussar data.

Processing and analysis of data recorded from a buried permanent seismic source

Tyler W. Spackman*† and Don C. Lawton

ABSTRACT

The Containment and Monitoring Institute and the University of Calgary have established a Field Research Station (FRS) in Newell County, Alberta for the purpose of testing various monitoring technologies to advance monitoring technologies for carbon sequestration projects. This paper investigates initial data acquired by a buried, permanent seismic source for rapid time-lapse seismic surveys. The source is a linear orbital vibrator manufactured by GPUSA. For this project it was cemented into a borehole at depth of 15 m below surface. The maximum frequency of this source is 200 Hz.

Installation and initial testing of the permanent sources at the Field Research Station was performed in September 2018. This study describes the differences between the buried permanent sources installed at the FRS and a traditional surface vibratory source. Acquisition parameters used in the initial tests are evaluated in terms of up-sweep and down-sweep time duration and frequency range. The paper will show the results of these initial tests, with a focus on the borehole source, and will comment on some of the unique considerations for permanent source data.

Raw correlated permanent source data exhibit a ringy character due to the ω^2 power spectrum. After applying Gabor deconvolution to the correlated data, the down-going and up-going wavefields are more easily identifiable, and image is comparable, if not superior to, those from a more conventional Vibroseis source at the ground surface, as shown in Figure 1.

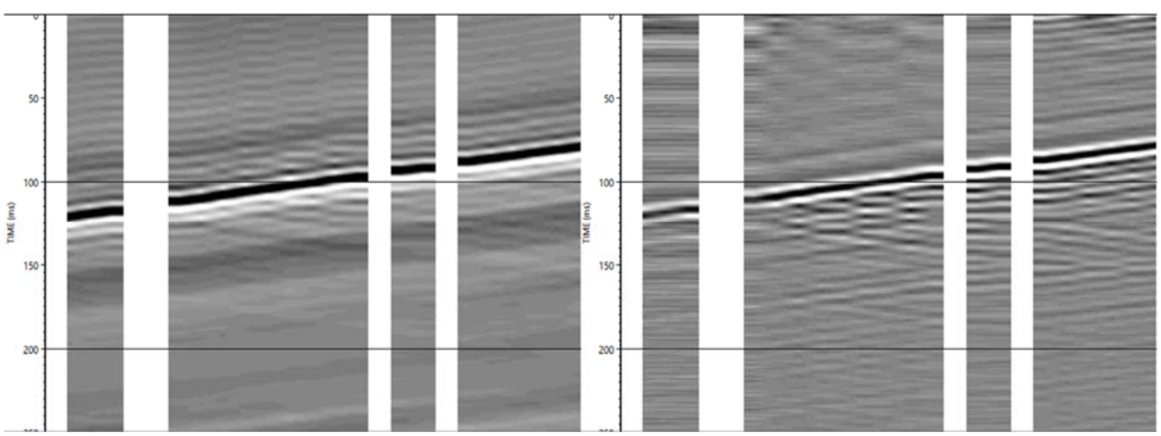

FIG. 1. VSP data acquired with Vibroseis source (left) and a GPUSA buried permanent seismic source (right). Gabor deconvolution has been applied to both records. White stripes are noisy geophones that were nulled for this display.

Elastic modeling and reverse time migration

Ziguang Su† and Daniel Trad

ABSTRACT

In an elastic medium, reverse time migration uses the velocity-stress method for the wavefield propagation to create synthetic shot records, which needs a numerical seismic source. This report discusses different ways to introduce a seismic source in the elastic modeling process. The seismic source in the elastic reverse time migration/RTM is normally expressed by a combination of wavelet functions in spatial and time dimensions. In most occasions, pure P/S wave sources are preferred. This paper shows that the typical way to form a source is not a pure P/S wave source. Then a new way of using a plate source to form a pure P/S wave source is introduced. Utilizing an elastic modeling process, a shot record can be created that contains all the information on P&S wave velocity and density. Acoustic RTM and acoustic least squares reverse time migration/LSRTM are employed to generate a reflectivity model. The output of S wave acoustic RTM is not satisfying but the LSRTM produces a clean image of S wave velocity because it has the ability to filter the unwanted events if the correct velocity model is given.

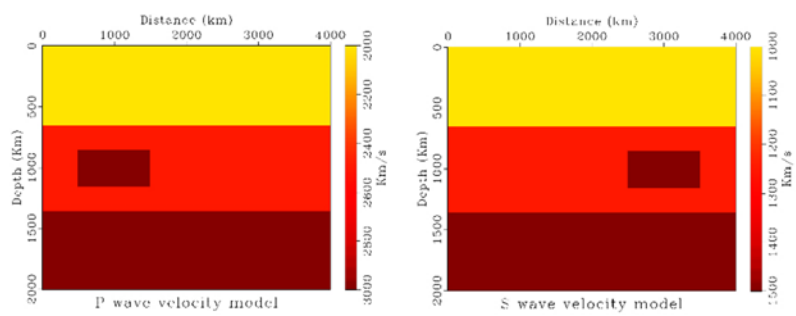

FIG. 1. P and S wave velocity model

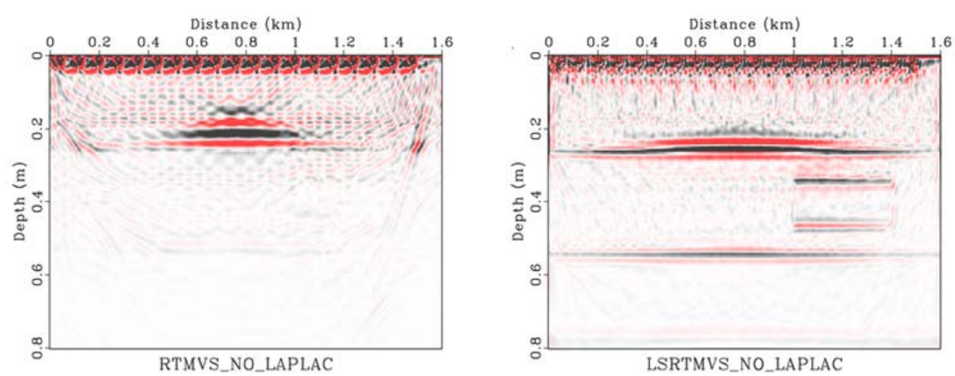

FIG. 2. The RTM and LSRTM outputs from rotation shot records. They both contain PS and SS images. PP waves exists on the top of the image.

A deep learning perspective of the forward and inverse problems in exploration geophysics

Jian Sun*†, Zhan Niu, Kris Innanen, Junxiao Li*, and Daniel Trad

ABSTRACT

Deeping learning has become a very powerful and efficient technique in many fields, where the recurrent neural network (RNN) has significant benefits of exhibiting temporal dynamic behavior for time dependency tasks by building a directed graph of a sequence. In this paper, with a self-designed RNN framework, the forward modeling of wave propagation is casted into a forward propagation of RNN, which allows the inversion problem being treated as the training process of RNN. Using this specific network, we numerically analyze the influence and playing role of learning rate (i.e., step-size) for each gradient-based optimization algorithm. Comparisons of gradient-based and non-linear algorithms are also discussed and anlyzed. To examine our analysis, the Marmousi model is employed to perform the inversion on the proposed RNN using both gradient-based and non-linear algorithms.

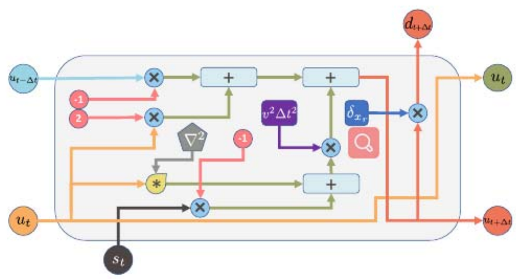

FIG. 3. Designed architecture of one single cell in RNN.

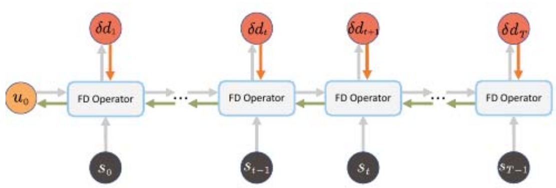

FIG. 4. The unrolled acyclic graph of RNN for back-propagation.

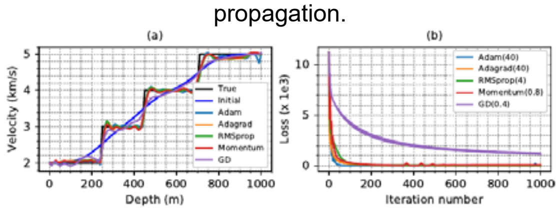

FIG. 11. Comparisons of best performances using gradient-based algorithms.

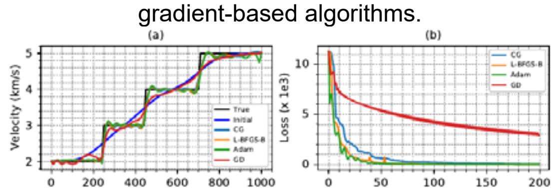

FIG. 15. Comparisons of best performances using GD, Adam, CG, and L-BFGS algorithms.

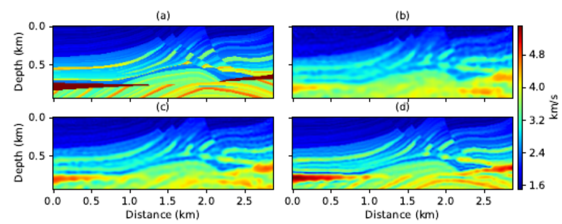

FIG. 18. Inversion with Adam at [True, 25th,50th,100th].

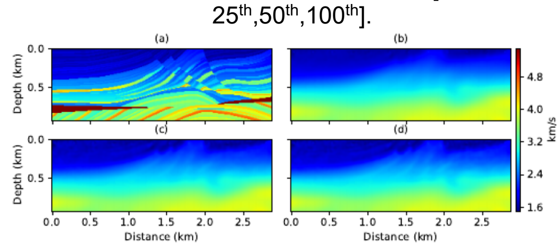

FIG. 19. Inversion with CG at [True, 100th,200th,300th].

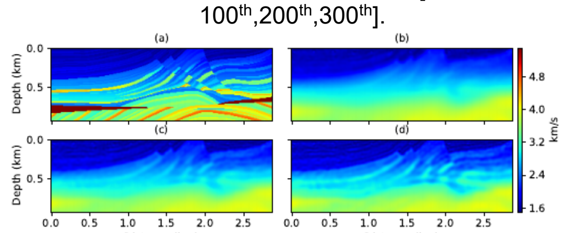

FIG. 20. Inversion with L-BFGS at [True, 100th,200th,300th].

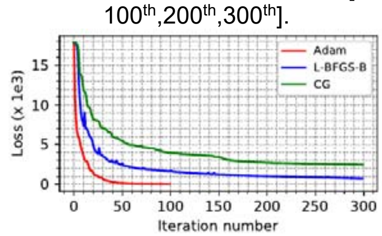

FIG. 21. Comparisons of Adam, CG, and L-BFGS algorithms on Marmousi model.

Assumptions and goals for least squares migration

Daniel Trad† and Sam Gray

ABSTRACT

Least squares migration (LSMIG) uses the assumption that if we have an operator that can create data from a reflectivity function, the optimal image will predict the actual recorded data with minimum square error. For this assumption to be true, it is also required that: a) the prediction operator must be error-free; b) model elements not seen by the operator should be constrained by other means; c) data weakly predicted by the operator should make limited contribution to the solution. Under these conditions, LSMIG has the advantage over simple migration of being able to remove interference between different model components. LSMIG does that by deconvolving or inverting the so-called Hessian operator. The Hessian is the cascade of forward modeling and migration; for each image point, it computes the effects of interference from other image points (point-spread function) given the actual recording geometry and the subsurface velocity model. Because the Hessian contains illumination information (along its diagonal), and information about the model cross-correlation produced by non-orthogonality of basis functions, its inversion produces illumination compensation and increases resolution. In addition, sampling deficiencies in the recording geometry map to the Hessian (both diagonal and non-diagonal elements), so LSMIG has the potential to remove sampling artifacts as well. These (illumination compensation, resolution, mitigating recording deficiencies) are the three main goals of LSMIG, although the first one can be achieved by cheaper techniques. To invert the Hessian, LSMIG relies on the residual errors during iterations. Iterative algorithms, like conjugate gradient and others, use the residuals to calculate the direction and amplitudes (gradient and step size), of the necessary corrections to the reflectivity function or model. Failure of conditions a), b) or c) leads the inversion to calculate incorrect model updates, which translate to noise in the final image.

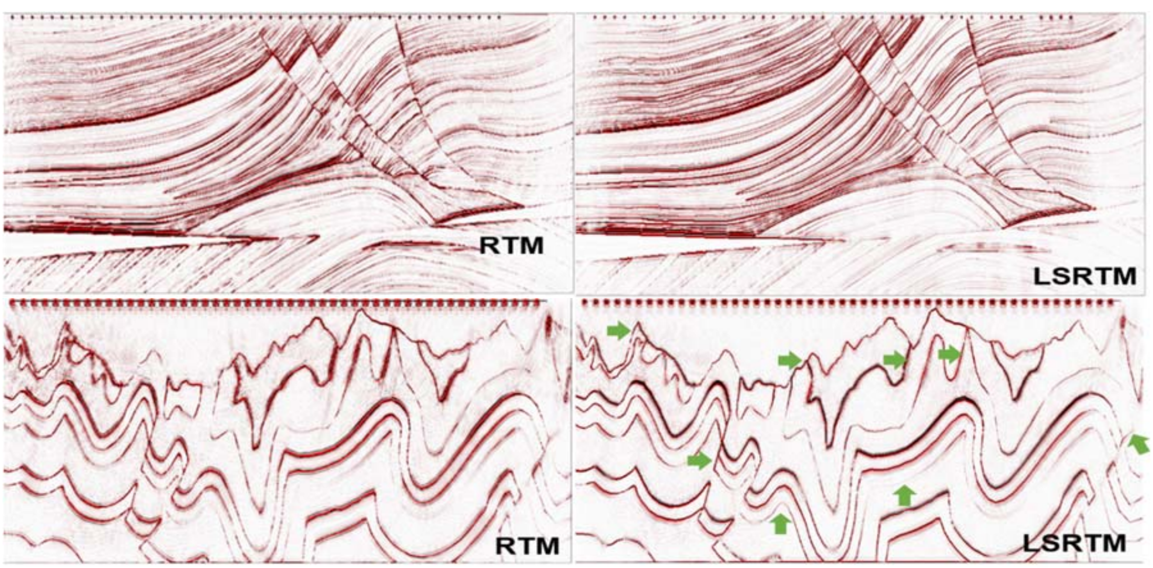

FIG. 1. RTM and LSRTM for Marmousi and Amoco models using 9 iterations and 50 shots.

Compressive sensing, sparse transforms and deblending

Daniel Trad*

ABSTRACT

Data acquisition is by far the most expensive and problematic part of seismic methods. In particular, 3-dimensional data surveys always have deficient sampling in at least 2 of the 4 spatial dimensions. As a consequence, geophysicists make extensive efforts in the mitigation of sampling problems. These efforts usually involve two directions: data interpolation and simultaneous acquisition. Interpolation is intended to create new seismic traces from the acquired samples by using sparse transformations. Simultaneous acquisition, also known as blending, attempts to mitigate the sampling problem by acquiring more data without increasing the acquisition cost. Simultaneous acquisition is a very cost-effective approach that reduces the cost of seismic information in both marine and land settings. Its main difficulty is the processing of the resulting seismic data, which requires shot separation or deblending, very early in the signal processing chain.

In the last few years, the two approaches have been merged in geophysics with the name of Compressive Sensing (CS). CS refers to an approach developed in the field of mathematics, which permits to obtain information with less sampling by relying on the combination of irregular sampling and sparseness to extract information from sparsely sampled data. CS involves acquiring data in a random fashion, using simultaneous sources, and performing deblending and denoising right at the beginning of processing by using sparse transforms.

In this report, I will discuss the relationships between CS and sparse transforms, showing that both are just the same approach with different name. Then, I will discuss one particular approach for deblending based on migration/demigration as the transform method. Finally, I will consider the merge of 5D interpolation with LSMIG as a single approach for deblending.

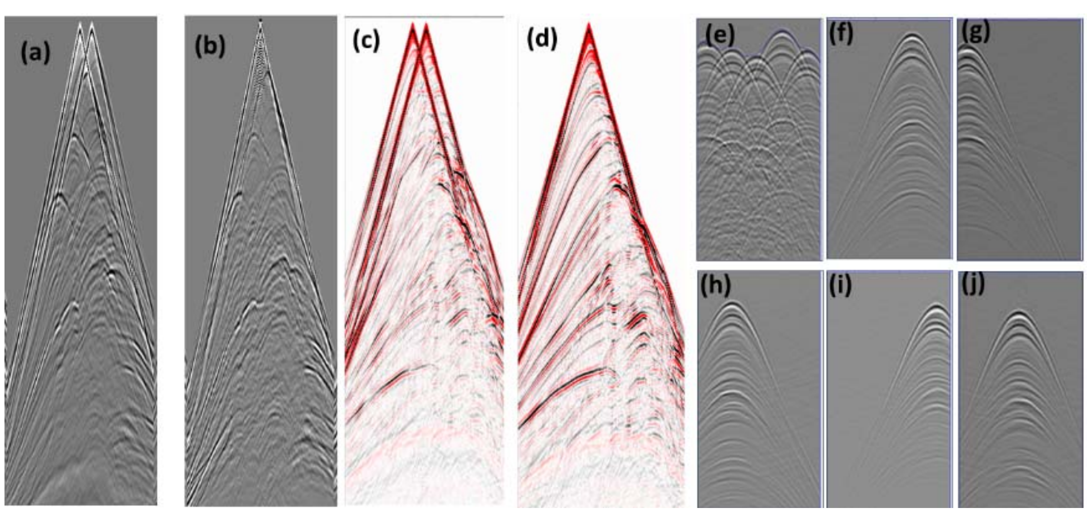

FIG. 1. Deblending through different migration algorithms: a-b: Kirchhoff, c-d: RTM, e-j: Apex-shifted Radon (Stolt migration).

Can continuously recorded seismic data be improved with signal processing? The application of deconvolution to microseismic data

Ronald Weir[†], Larry Lines, and Don C. Lawton

ABSTRACT

Passive seismic recording is increasingly being used to record seismic events associated with hydraulic fracture stimulation. The recorded amplitudes of these induced seismic events are relatively small and may be undetectable given the noisy environment in which they are recorded. Here we describe a method using reflection seismic processing techniques applied to continuously recorded passive (microseismic) data. Signal processing has been used for many years in reflection seismic processing to enhance signal quality. Algorithms such as deconvolution, scaling, and various types of filtering have been routinely applied to raw recorded data to enhance the processing and interpretability of the recorded data. Induced seismic events, such as perforation shots, can provide a time to depth relationship, although they may be difficult to detect. Induced seismic events caused by hydraulic fracturing events can indicate the depth and direction of the fracture stimulation, and induced seismicity may identify geohazards. In this study we apply a combination of the more commonly used algorithms used in reflection data processing to continuously recorded microseismic data and demonstrate how signal quality can be improved. These results demonstrate how signal processing can lead to more reliable detection of induced seismic events, and significantly improve the overall signal quality.

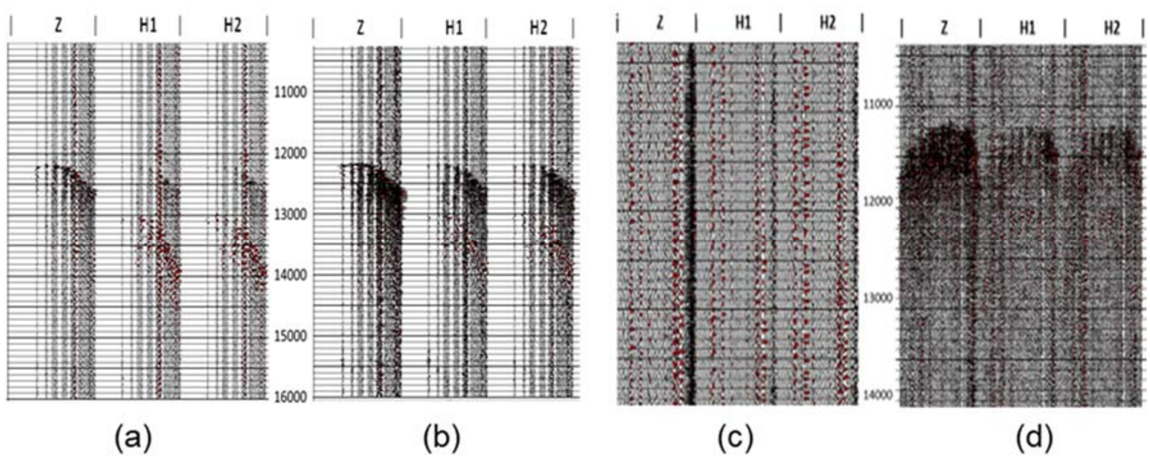

FIG. 1. Examples of raw data, and conditioned data. (a) raw 6 second record showing vertical (z)and horizontal H1,H2 components sorted in terms of offset; (b) the same record after deconvolution (c) example of a noisy record, and (d) shows how data conditioning using deconvolution can enhance the signal to noise ratio.

Focal-time estimation: A new method for stratigraphic depth control of induced seismicity

Ronald Weir*, Andrew Poulin, Nadine Igonin, David W. Eaton, Larry Lines, and Don C. Lawton

ABSTRACT

In this paper we describe a novel method for focal-depth determination of induced seismic events. Our approach involves joint interpretation of microseismic and induced-seismicity waveform observations along with multicomponent surface seismic data. The method operates using parallel workflows for processing induced-seismicity data and P-P and P-S data. The output is a set of calibrated P-P times for the microseismic events, which thereby enables the events to be co-rendered and visualized with the seismic data, thus providing stratigraphic control on source locations. The method requires Vp and Vs time-depth control from coincident multicomponent seismic data and is achieved by registration of P-P and P-S reflections from equivalent horizons. Hypocenter vertical locations are initially expressed as the zero-offset focal time (2-way P-P reflection time) and then converted to depth by leveraging methods available for time-depth conversion of the surface seismic data, as well as well ties using synthetic seismograms. Application of this method requires high-quality P- and S-wave picks for microseismic events, which are extrapolated to zero offset. This approach avoids the necessity to build and calibrate a 3-D velocity model for hypocenter location, nor determination of accurate absolute origin times. This method also implicitly accounts for factors that are often ill-constrained for most velocity models, e.g. velocity anisotropy, since these factors similarly affect both the induced seismicity and the 3-D seismic travel times. We apply our new method to an induced seismicity dataset with events up to M_L3.6, recorded using a shallow-well monitoring array in Alberta, Canada. Reconciling the seismic processing datum with the microseismic datum was found to be a critical, but not insurmountable, challenge. The inferred focal depths place most induced events at, or above, the treatment depth.

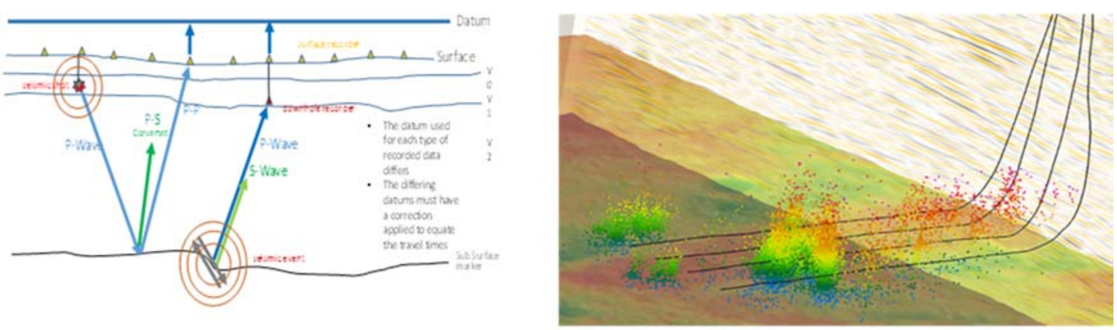

FIG. 1. Illustration of the relationship between recorded seismic data and microseismic recording. Reflection seismic data is corrected to an artificial datum, above the highest elevation. The Dark arrows represent PP (reflection), P direct, the grey arrows represent P-S (reflection) and S direct (microseismic). The reflection seismic data is time-adjusted downward to match the microseismic data. The 3-D rendered image shows the calculated hypocenter depths with the well trajectories, inserted into the depth-converted 3-D volume.

Comparison between time domain and frequency domain least-squares reverse time migration

Lei Yang† and Daniel Trad

ABSTRACT

We compare the algorithms of least-squares reverse time migration (LSRTM) in both time and frequency domain and propose a full waveform inversion (FWI) based LSRTM method in the frequency domain. We first prove that the gradient of the FWI objective function is equivalent to the reverse time migration (RTM) imaging condition. Using the truncated Newton method, we solve the linear equation which relates Hessian, model perturbation and the gradient by linear conjugate gradient method. We use a 2-layer model to compare LSRTM in time and frequency domain and find that the images are both accurate when the initial model is accurate. However, when the initial model is inaccurate, the reflector depth is not correct for the time domain LSRTM. In contrast, the FWI-based LSRTM method can produce an accurate reflector depth when the initial velocity is not accurate, which indicates that the FWI-based LSRTM is more robust when the initial model is inaccurate.

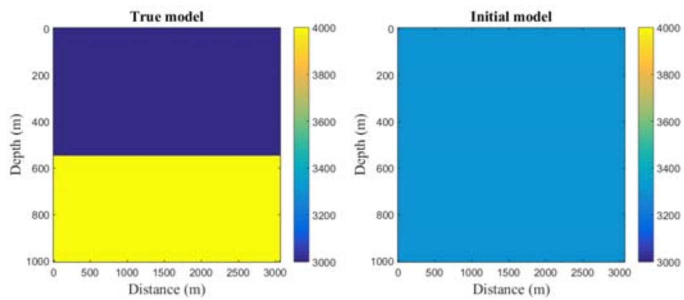

FIG. 1. The True model and the initial model with wrong velocity.

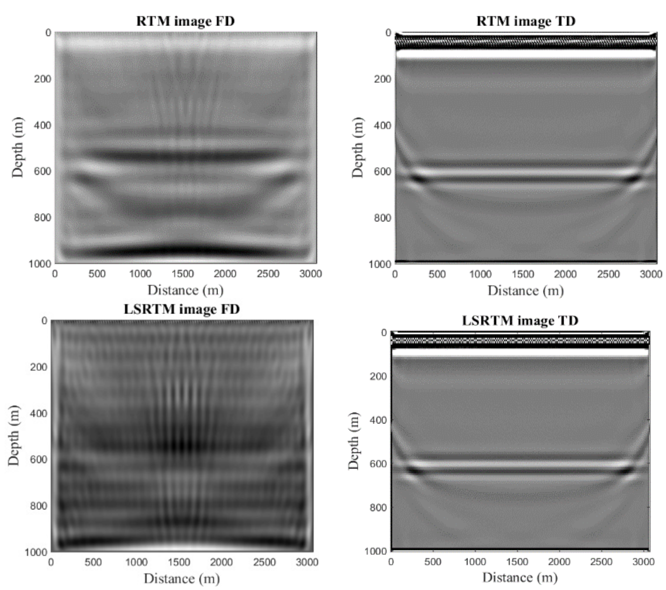

FIG. 2. Comparisons between time and frequency domain RTM and LSRTM with different initial model.

CREWES Sponsors Meeting 2018

Presentation Schedule

Thursday November 29, 2018

TIME	SESSION Moderator	TITLE	SPEAKER
8:30	**ACQ / Innanen**	Welcome and new developments at CREWES	Kris Innanen
8:50		A shear wave land streamer	Don Lawton
9:10		CREWES 2018 simultaneous 3C / DAS WVSP field experiment	Kevin Hall
9:30		Design and deployment of a multicomponent DAS sensor	Kris Innanen
9:50		Microseismic and SWD in the physical modelling lab	Nadine Igonin
10:10		Compressive sensing, de-blending & a new dataset	Daniel Trad
10:30		***Break***	
11:10	**MON / Lawton**	Monitoring with permanent source data	Tyler Spackman
11:30		Ambient noise monitoring at CaMI-FRS	Marie Macquet
11:50		Monitoring methane gas migration in the near surface	Tim Cary
12:10		***Break – Lunch***	
1:30		A proposal for & applications of a marine thermal probe	Rachel Lauer
1:50		Results from 2018 CaMI DAS VSP data acquisition	Heather Hardeman
2:10		Inversion for stress & fluids in randomly-oriented fractures	Huaizhen Chen
2:30	**PROC / Lines**	Wrinkle reduction in 3D source ensembles	David Henley
2:50		***Break***	
3:10		A method for stratigraphic depth control of induced seismicity	Ron Weir
3:30		Processing of walkaway DAS / geophone VSP data	Adriana Gordon
3:50		Internal multiple prediction and generator spectra	Andrew Iverson
4:10-5:45	**POSTERS**	Posters	

Friday November 30, 2018

TIME	SESSION Moderator	TITLE	SPEAKER
8:30	**LFWI / Innanen**	Log-validated FWI with wavelet phase & amplitude updating	Sergio Romahn
8:50		Viscoelastic FWI: solving for Q_P, Q_S and V_P, V_S and density	Scott Keating
9:10		Towards 4C FWI: DAS and 3C as complementary datasets	Matthew Eaid
9:30		Practical multicomponent land FWI	Raul Cova
9:50		***Break***	
10:30		Connecting FWI and LSRTM through variable restriction	Scott Keating
10:50	**ML / Trad**	Deep learning and FWI	Jian Sun/Junxiao LI
11:10		Machine learning for facies classification & target identification	Marcelo Guarido
11:30		Velocity model building with slope tomography	Bernie Law
11:50		***Break - Lunch***	
1:00		P- and S-wave elastic reverse time migration	Jorge Monsegny
1:20	**NI / Lawton**	The next generation of drillstring imaging techniques	Roman Shor
1:40		Least squares RTM of a seismic-while-drilling dataset	Nasser Kazemi
2:00		***Break***	
2:20		Geophysics and medicine in symbiosis	Larry Lines
2:40		Quantum computing in exploration / monitoring seismology	Shahpoor Moradi
3:00		New monitoring modes: time boundaries & elastic bracing	Kris Innanen
3:20		Deep neural networks to predict reservoir properties	Jon Downton

ACQ Acquisition & sensing	MON Monitoring	PROC Processing, DAS and multiples	Posters	LFWI Practical land FWI in the reservoir	ML Machine learning & Imaging	NI New ideas & seismic applications